



Assessments of Nitrate Budgets in the Yellow Sea Based on a 3D Physical-Biogeochemical Coupled Model

Yong-Jin Tak^{1,2}, Yang-Ki Cho^{1*}, Jeomshik Hwang¹ and Yong-Yub Kim¹

¹ School of Earth and Environmental Sciences, Research Institute of Oceanography, Seoul National University, Seoul, South Korea, ² Department of Atmospheric Sciences, Yonsei University, Seoul, South Korea

OPEN ACCESS

Edited by:

Zhiyu Liu,
Xiamen University, China

Reviewed by:

Peng Xiu,
South China Sea Institute
of Oceanology, Chinese Academy
of Sciences (CAS), China
Jie Shi,
Ocean University of China, China

*Correspondence:

Yang-Ki Cho
choyk@snu.ac.kr

Specialty section:

This article was submitted to
Physical Oceanography,
a section of the journal
Frontiers in Marine Science

Received: 29 September 2021

Accepted: 27 December 2021

Published: 18 January 2022

Citation:

Tak Y-J, Cho Y-K, Hwang J and
Kim Y-Y (2022) Assessments
of Nitrate Budgets in the Yellow Sea
Based on a 3D
Physical-Biogeochemical Coupled
Model. *Front. Mar. Sci.* 8:785377.
doi: 10.3389/fmars.2021.785377

Nitrate (NO_3^-) plays an important role in ecosystems and aquaculture in the Yellow Sea (YS). Sparse observational data suggest that ocean currents and nitrification are crucial to NO_3^- flux in the YS; however, a quantitative assessment of these fluxes has not yet been performed. This study investigates seasonal and spatial variations in NO_3^- flux via currents and biological processes in the YS from 2006 to 2019 using a physical-biogeochemical coupled model. The model results show that the current-driven fluxes exceeded biological processes in the eastern and central regions of the YS, unlike in the western and northern regions. Advection of NO_3^- in the YS is mainly driven by cyclonic circulation in summer and fall, and anticyclonic circulation in spring and winter. The Subei Coastal Current along the coast of China plays a primary role in net advective influx of NO_3^- to the YS year round. The NO_3^- influx by the Yellow Sea Warm Current along the lower layer of the southcentral YS is offset by outflux through wind-driven surface currents in winter. The southward movements of the Yellow Sea Bottom Cold Water in summer and the Korean Coastal Current in winter are major NO_3^- outfluxes to the East China Sea. In terms of biological processes, NO_3^- is mainly consumed by phytoplankton during the spring bloom and supplied through organic matter decomposition and nitrification. Net supply of NO_3^- by biological processes was the greatest in the southcentral YS where the Yellow Sea Bottom Cold Water is present.

Keywords: nitrate flux, physical-biogeochemical coupled model, Yellow Sea, nitrification, advective flux of nitrate

INTRODUCTION

The Yellow Sea (YS) in the Northwestern Pacific Ocean is a shallow, semi-enclosed marginal sea with an average depth of approximately 50 m and a deep trough (>90 m) in its center (Figure 1). The YS is a typical marginal sea with high primary productivity and rich fishery resources. Dissolved inorganic nitrogen (DIN) including nitrate (NO_3^-), nitrite (NO_2^-), and ammonium (NH_4^{++}) is critical in biological production and often a limiting factor in primary production in marine ecosystems (Ryther and Dunstan, 1971; Howarth, 1988). The fixed nitrogen in the YS is supplied by various sources including advection, rivers, atmospheric deposition, sediment flux, and nitrogen fixation (Bashkin et al., 2002; Kim et al., 2011; Kim S. K. et al., 2013). Previous studies reported that NO_3^- , accounting for approximately 87% of the total inorganic nitrogen in the YS, is the most

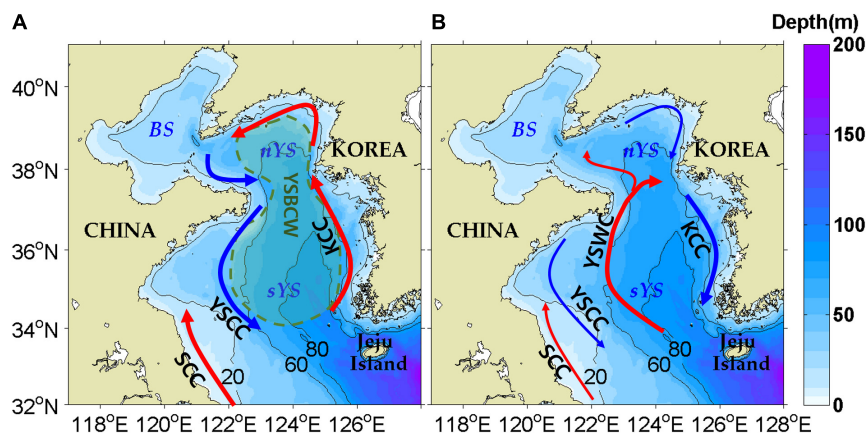


FIGURE 1 | Schematic diagrams of ocean currents during summer (A) and winter (B) in the Yellow Sea. KCC, SCC, YSCC, YSBCW, YSWC, BS, nYS, and sYS indicate the Korean Coastal Current, Subei Coastal Current, Yellow Sea Coastal Current, Yellow Sea Bottom Cold Water, Yellow Sea Warm Current, Bohai Sea, northern Yellow Sea, and southern Yellow Sea, respectively.

important species of fixed nitrogen for primary production and aquaculture in the YS (Fu et al., 2009; Jin et al., 2013; Liu et al., 2017).

Seaweed aquaculture is an important industry in the coastal area of the YS during winter (Chengkui, 1984; Kim et al., 2017; Park et al., 2018). The chlorosis presumably caused by NO_3^- depletion has frequently damaged the aquaculture industry along the Korean coast since 2010 (NFRDI, 2014; Shim et al., 2014). At the same time, eutrophication has caused significant algal blooms along the coast of China, having negative impacts on fishery resources (Liu et al., 2013; Li et al., 2015).

Several studies have investigated NO_3^- flux in the YS using a range of methods (Liu et al., 2003; Wu et al., 2019; Guo et al., 2020). Liu et al. (2003) quantified nutrient fluxes using a single box model but did not consider the effect of currents and *in situ* biological processes (e.g., nitrification and NO_3^- uptake by phytoplankton). Wu et al. (2019) reported the importance of nitrification for NO_3^- flux in the YS using isotope analysis without quantitative assessment. Guo et al. (2020) showed the effects of physical and biological processes in the southern YS focusing on three different regions. Riverine input, atmospheric deposition, anthropogenic input, and flux from sediments have been suggested as NO_3^- sources in the YS (Bashkin et al., 2002; Lim et al., 2008; Li et al., 2015). However, the effect of advection by currents has not yet been quantitatively assessed.

Circulation in the YS is dominated by the East Asian Monsoon system. In summer, cyclonic circulation occurs due to the baroclinic effect of strong solar radiation and river inputs to the YS, and the northward Subei Coastal Current (SCC) occurs along the Chinese coast (Figure 1A; Yanagi and Takahashi, 1993; Hwang et al., 2014; Yuan et al., 2017; Wu et al., 2018; Xing et al., 2020). In winter, the Yellow Sea Warm Current (YSWC) is the dominant flow due to the northwesterly monsoon (Uda, 1934; Hsueh, 1988; Beardsley et al., 1992; Teague and Jacobs, 2000; Lie et al., 2001; Lin et al., 2011; Tak et al., 2016). The northwesterly wind also generates southward downwind flows known as the Korean Coastal Current (KCC)

and Yellow Sea Coastal Current (YSCC) (Figure 1B). The northward YSWC turns eastward off the Shandong Peninsula and connects to the southward KCC, resulting in anticyclonic circulation (Yanagi and Takahashi, 1993; Lin and Yang, 2011; Tak et al., 2020).

Transport via these various currents can influence the seasonal distribution of nutrients in the YS. The YSWC reportedly plays an important role in spring bloom by providing external nutrients to the YS (Hyun and Kim, 2003; Fu et al., 2009; Xuan et al., 2011; Jin et al., 2013; Zhou et al., 2013; Liu et al., 2015a,b; Guo et al., 2020). Zhou et al. (2013) reported that wind speed is significantly correlated with the spring bloom by intensifying the nutrient-carrying YSWC in the deep layer. Some sparse observations also implied that the YSWC provides relatively high amounts of nutrients to the phytoplankton community (Jin et al., 2013; Liu et al., 2015a). In addition to the YSWC, the KCC, YSCC, and SCC may also affect nutrient distributions via physical transport.

The Yellow Sea Bottom Cold Water (YSBCW) likely stores the nutrients supplied by organic matter decomposition (Hyun and Kim, 2003; Jang et al., 2013; Wei et al., 2016; Fu et al., 2018; Wu et al., 2019; Guo et al., 2020). Wu et al. (2019) argue that nitrification is the major biological process in the interior of the YSBCW resulting in increased NO_3^- concentration from spring to fall. The accumulated NO_3^- in the YSBCW is supplied to the surface layer through vertical mixing by wind and cooling in winter. In addition, the YSBCW may transport NO_3^- southward from the YS to the East China Sea (ECS) by upwind flow in summer (Yang et al., 2014).

The effects of the currents and biological processes on NO_3^- fluxes are yet to be quantitatively investigated. Moreover, the distinct seasonal differences in the circulation and hydrography in the YS warrant further investigation. Using a three-dimensional (3D) physical-biogeochemical coupled numerical model, this study aimed to quantitatively deconvolute the NO_3^- flux in the YS to advective transport by currents and biological process.

MATERIALS AND METHODS

Data and Model Configuration

The physical numerical model applied for the study was the Regional Ocean Modeling System (ROMS), a free-surface model with horizontally curvilinear and vertically terrain-following coordinates that solves hydrostatic, incompressible, primitive equations (Shchepetkin and McWilliams, 2005). The model domain ranged zonally from 117.5 to 130.3°E and meridionally from 24.8 to 41.0°N including the ECS and YS (Figure 2A). Bottom topography data were derived from Kim C. -S. et al. (2013). The model grid resolution was approximately 1/30 degrees horizontally and 40 sigma layers vertically.

The horizontal advection scheme used third-order upstream advection. The horizontal harmonic mixing scheme and the K-Profile parameterization scheme were applied (Large et al., 1994). For the lateral open boundary, monthly mean temperature, salinity, sea surface height, and velocity data were obtained from the Northwestern Pacific Model (Seo et al., 2014). For the surface forcing data, six-hourly wind, air temperature, sea level pressure, relative humidity, daily solar radiation, and precipitation datasets were obtained from the ERA5 reanalysis data of the European Centre for Medium-Range Weather Forecasts (Copernicus Climate Change Service, 2017). The surface heat flux was calculated using bulk formulae (Fairall et al., 1996).

Tidal forcing of 10 tidal components obtained from TPXO6 was imposed at the lateral boundaries of the model (Egbert and Erofeeva, 2002). Monthly mean river discharge was applied for 12 rivers in the BS and YS, freshwater discharge from the Changjiang River was observed at the Datong station, discharge data for Han and Geum Rivers along the eastern coast of the YS were derived from the National Institute of Environmental Research (NIER), and discharge data for all other rivers along the Chinese and Korean coasts were obtained from the Global River Discharge Database (Vörösmarty et al., 1996; Wang et al., 2008). The initial temperature and salinity for an experiment were obtained

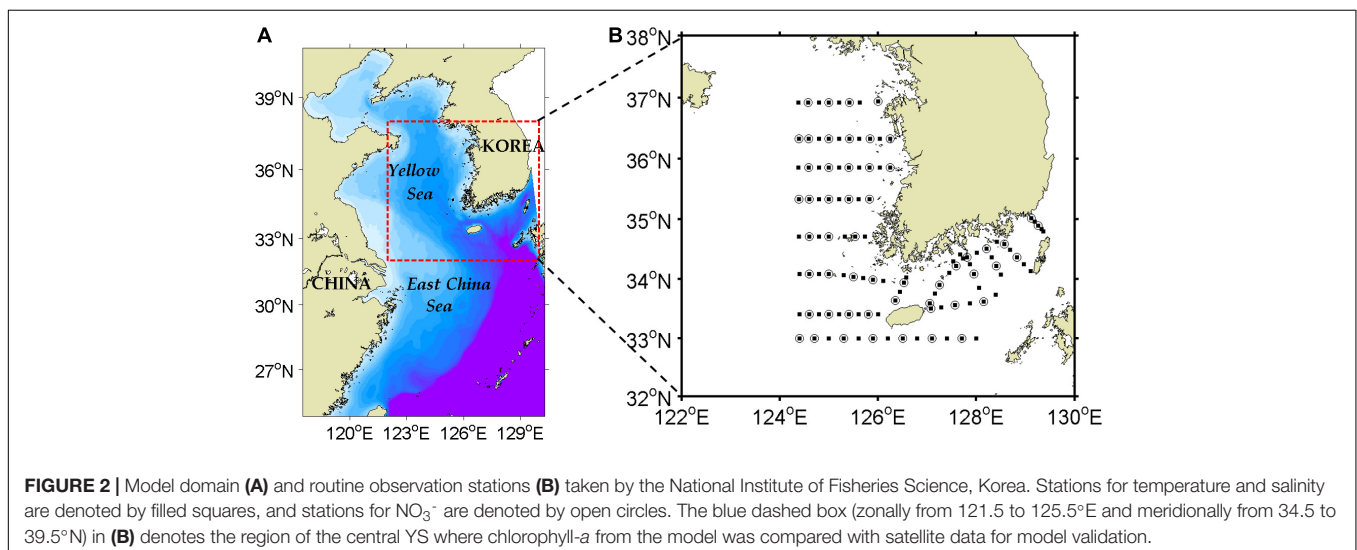
from the National Ocean Data Center World Ocean Atlas 2013 (WOA2013) (Locarnini et al., 2013; Zweng et al., 2013). The initial velocity field was calculated by the geostrophic equation using the initial temperature and salinity.

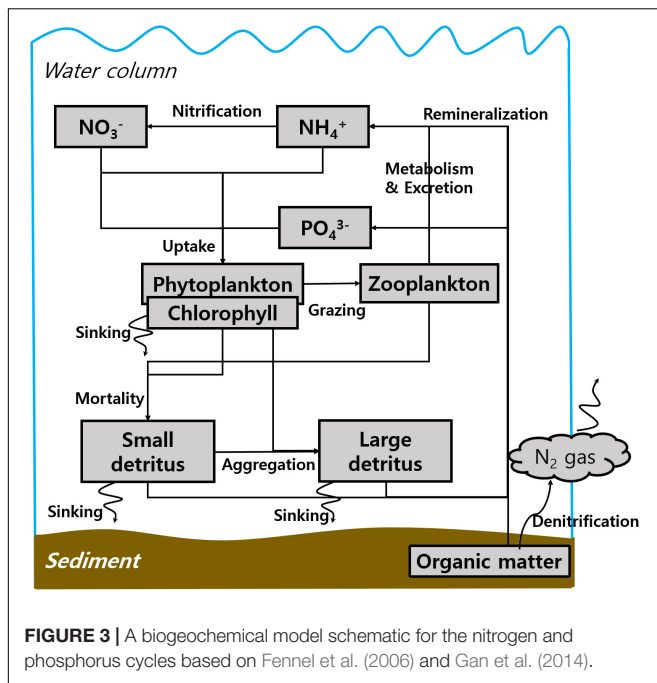
Primary production in the YS is not limited by silicate but by nitrogen or phosphorus (Wang et al., 2003; Jin et al., 2013). Thus, a biogeochemical model based on the nitrogen and phosphorus cycles is appropriate for simulating the biogeochemical environment in the YS. The biogeochemical model coupled with the physical model is based on the nitrogen and phosphorus cycles described by Fennel et al. (2006) and Gan et al. (2014). A schematic diagram for the biogeochemical model is shown in Figure 3. The scheme includes the following 10 prognostic variables: phytoplankton, chlorophyll-*a*, zooplankton, small nitrogen detritus (SDN), small phosphorus detritus (SDP), large nitrogen detritus (LDN), large phosphorus detritus (LDP), NO_3^- , NH_4^+ , and phosphate (PO_4^{3-}).

The growth of phytoplankton depends on temperature, radiation, and nutrient concentrations, and radiation is attenuated by water and chlorophyll-*a* concentrations. The attenuation coefficient by water (K_w) was set to 0.09 m^{-1} in the entire model domain, which is higher than the model default value (0.04 m^{-1}) because the turbidity in the YS is considerably high (Shi and Wang, 2012). According to prior studies, the light attenuation coefficient (K_d), which is calculated by the sum of the K_w and multiplying the light attenuation coefficient for chlorophyll-*a* (K_{chl}) by the integration of chlorophyll-*a* in the water column in the biogeochemical model, can be estimated by an empirical equation as follows (Holmes, 1970; Castillo-Ramírez et al., 2020):

$$K_d = 1.4/Z_{SD}, \quad (1)$$

where Z_{SD} denotes the Secchi disk depth. *In situ* observation by the National Institute of Fisheries Science (NIFS), Korea, showed that the annual mean Z_{SD} was 10 m at the central stations and 5 m at the coastal stations in the YS. Thus, K_d in the central and coastal stations can be estimated as 0.14 and 0.28 m^{-1} ,





respectively. However, because the Secchi disk depth includes an attenuating effect of phytoplankton and the model domain is based on open ocean, we performed several sensitivity tests for evaluating a reasonable attenuation coefficient and selected 0.09 m^{-1} as an adequate value in the YS.

Uptakes of NO_3^- , NH_4^+ , and PO_4^{3-} are estimated by Michaelis–Menten equations with preferential consumption of NH_4^+ in the nitrogen uptake by phytoplankton (Menten and Michaelis, 1913). The model assumed that organic matter decomposition was converted to inorganic nutrients as soon as the organic matter reached the bottom layer because approximately 90% of the organic matter derived from primary production is mineralized in the water column (Song et al., 2016). In other words, sediment nutrient flux into the bottom layer was employed without a time lag because only 10% of the organic matter could reach the sediment. Since most of the organic matter should be remineralized before reaching the bottom layer in the YS, the small and large detritus remineralization rates were set to 0.04 and 0.02 d^{-1} , respectively. Fennel et al. (2006) estimated that 14% of organic matter decomposition involved denitrification in the Mid-Atlantic Bight region. However, we assumed that 9% of the decomposition was denitrified because the YS maintained a sufficient level of oxygen to suppress denitrification and the organic matter content in the surface sediment was low, indicating that biological processes in the sediment may play a secondary role in the YS (Zhao et al., 2018; Wu et al., 2019).

The velocities of large detritus, small detritus, and phytoplankton were set to 2.0, 0.2, and 0.1 m d^{-1} , respectively, which were within the range of general sinking velocities in the ocean based on observation, the Stokes equation, and sensitivity model analyses considering the size and density of a particle (Smayda, 1969; Fasham et al., 1990; Moskilde, 1996). In addition

to particle characteristics, sinking velocity can also be regulated by seawater density. Thus, the empirical equation for vertical sinking velocities of phytoplankton and detritus was modified depending on temperature (as the main control of the seawater density) as per Bach et al. (2012). Accordingly, the sinking velocity doubled as the temperature increased by 15°C at a salinity of 35 g kg^{-1} . Considering the salinity variation from 29 to 34 g kg^{-1} in the YS, the velocity equation in the model was modified to increase with temperature more rapidly as follows:

$$\begin{cases} W_p = \frac{W_d}{3} (T < 10^\circ\text{C}) \\ W_p = \frac{W_d}{3^{-2\left(\frac{T-10}{15}\right)}} (10 \leq T \leq 25^\circ\text{C}) \\ W_p = W_d (T > 25^\circ\text{C}) \end{cases} \quad (2)$$

where T is temperature, and W_p and W_d are the particle sinking velocity under the temperature-varying condition and the default value of the velocity, respectively.

Several biological parameters related to primary production, such as the initial slope of the photosynthesis-irradiance curve, maximum chlorophyll to phytoplankton ratio, half-saturation for phytoplankton of NH_4^+ uptake, phytoplankton and zooplankton mortality rates, zooplankton grazing rate, and zooplankton half-saturation constant for ingestion, were tuned properly for the YS environment to simulate the spring bloom and its magnitude. Further details on the nitrogen and phosphorus cycles in the biogeochemical model are described in Fennel et al. (2006) and Gan et al. (2014). The biogeochemical parameters applied in the model are provided in Table 1.

The initial and boundary conditions for chlorophyll-*a* in the water column were based on climatological monthly mean surface chlorophyll-*a* data obtained from the Moderate Resolution Imaging Spectroradiometer (MODIS)-aqua and an empirical model (Morel and Berthon, 1989; Uitz et al., 2006). The initial and boundary concentrations of NO_3^- and PO_4^{3-} were derived from the WOA 2013 dataset, and the concentration of NH_4^+ was set to $1\text{ }\mu\text{mol L}^{-1}$ as described by Garcia et al. (2013). The initial conditions of phytoplankton, zooplankton, and large and small detritus were estimated from the phytoplankton/chlorophyll-*a*, zooplankton/chlorophyll-*a*, and detritus/phytoplankton ratios of 0.5, 0.2, and 0.35, respectively (Gruber et al., 2006). The climatological annual mean concentrations of dissolved inorganic nitrogen and phosphorus in the 2000s, and the $\text{NO}_3^-/\text{NH}_4^+$ ratio for the Changjiang River, were applied in the model (Dai et al., 2011; Wang et al., 2011; Zhou et al., 2017). For the Yellow River, the annual mean concentrations of NO_3^- , NH_4^+ , and PO_4^{3-} for the period 2002–2004 were derived from Gong et al. (2015), and the respective concentrations in the Yalu River were obtained from Liu and Zhang (2004) for 1992, 1994, and 1996. The monthly mean riverine NO_3^- , NH_4^+ , and PO_4^{3-} inputs from the Korean Peninsula were obtained from the NIER. Constant atmospheric depositions of NO_3^- , NH_4^+ , and PO_4^{3-} of $0.027\text{ mmol N m}^{-2}\text{ d}^{-1}$, $0.080\text{ mmol N m}^{-2}\text{ d}^{-1}$, and $0.001\text{ mmol P m}^{-2}\text{ d}^{-1}$, respectively, were applied to the surface boundary conditions based on previous observations (Zhang, 1994; Li et al., 2015).

TABLE 1 | Biogeochemical model parameters used in this study and default values from Fennel et al. (2006).

Description	Symbol	Default value	Model value	Units
Phytoplankton growth rate at 0°C	μ_0	0.59	0.59	d^{-1}
Light attenuation due to seawater	K_{water}	0.04	0.09	m^{-1}
Light attenuation by chlorophyll	K_{Chla}	0.0249	0.0249	$(mg\ Chl)^{-1}\ m^2$
Initial slope of the P-I curve	α	0.125	0.03	$mgC\ gChl^{-1}\ (W\ m^{-2})^{-1}\ d^{-1}$
Maximum chlorophyll to phytoplankton ratio	θ_{max}	0.0535	0.075	$mgChl\ mgC^{-1}$
Half-saturation for phytoplankton NO_3^- uptake	k_{NO3}	0.5	0.5	$mmol\ N\ m^{-3}$
Half-saturation for phytoplankton NH_4^+ uptake	k_{NH4}	0.5	0.25	$mmol\ N\ m^{-3}$
Half-saturation for phytoplankton PO_4^{3-} uptake	k_{PO4}	–	0.17	$mmol\ P\ m^{-3}$
Cellular P:N ratio	r_{PN}	–	0.0625	Dimensionless
Phytoplankton mortality rate	m_p	0.072	0.1	d^{-1}
Zooplankton maximum grazing rate	g_{max}	0.6	0.83	$(mmol\ N\ m^{-3})^{-1}\ d^{-1}$
Zooplankton assimilation efficiency for nitrogen	β	0.75	0.75	Dimensionless
Zooplankton half-saturation constant for ingestion	k_p	1	2	$(mmol\ N\ m^{-3})^2$
Zooplankton-basal metabolism	l_{BM}	0.1	0.1	d^{-1}
Zooplankton-specific excretion rate	l_E	0.1	0.1	d^{-1}
Zooplankton mortality rate	m_Z	0.025	0.02	$(mmol\ N\ m^{-3})^{-1}\ d^{-1}$
Small detritus remineralization rate for nitrogen and phosphorus	r_{SD}	0.03	0.04	d^{-1}
Large detritus remineralization rate for nitrogen and phosphorus	r_{LD}	0.01	0.02	d^{-1}
Aggregation parameter	τ	0.005	0.005	$(mmol\ N\ m^{-3})^{-1}\ d^{-1}$
Sinking velocity for small detritus	w_{SDet}	0.1	0.2	$m\ d^{-1}$
Sinking velocity for large detritus	w_{LDet}	1.0	2.0	$m\ d^{-1}$
Sinking velocity for phytoplankton	w_{Phy}	0.1	0.1	$m\ d^{-1}$
Maximum nitrification rate	n_{max}	0.05	0.05	d^{-1}
Threshold PAR for nitrification inhibition	I_0	0.0095	0.0095	$W\ m^{-2}$
Half-saturation PAR for nitrification inhibition	k_I	0.036	0.036	$W\ ms^{-2}$

The coupled model was spun up for 7 years and was integrated for the period 2006–2019. To evaluate the performance of the model, the simulated temperatures, salinities, and NO_3^- concentrations in the YS were compared to bimonthly observational data obtained from the NIFS, Korea, for the corresponding period (Figure 2B). Data that deviated from the mean by more than one standard deviation were excluded from the analysis.

Estimation of Nitrate Flux

The temporal variation in NO_3^- concentrations is expressed as follows:

$$\frac{\partial [NO_3^-]}{\partial t} = (-\vec{u} \cdot \nabla [NO_3^-]) + (k_T \nabla^2 [NO_3^-]) + (-U_{NO_3} \cdot [Phyto]) + (L_{nitri} \cdot [NH_4^+]), \quad (3)$$

where $[NO_3^-]$, $[NH_4^+]$, $[Phyto]$, \vec{u} , k_T , U_{NO_3} , and L_{nitri} are the NO_3^- , NH_4^+ , and phytoplankton concentrations, three-dimensional velocity, diffusion, uptake rate of NO_3^- , and nitrification rate, respectively. The terms on the right side of the equation indicate advection, diffusion, NO_3^- uptake by phytoplankton, and nitrification, respectively. The first two terms are controlled by physical processes while the remaining terms are controlled by biological processes. The diffusion term was ignored in this study because it is almost negligible compared with the advection term. The effect of currents on NO_3^- flux

is reflected by the advection term. The uptake rate is defined as follows:

$$U_{NO_3} = \mu_{max} f(I) L_{NO_3}, \quad (4)$$

where μ_{max} , $f(I)$, and L_{NO_3} are the maximum growth rate, photosynthesis-light relationship, and half-saturation concentration for the uptake of NO_3^- , respectively. The maximum growth rate and photosynthesis-light relationship are defined as follows:

$$\mu_{max} = \mu_0 \cdot 1.066^T, \quad (5)$$

$$f(I) = \frac{\alpha I}{\sqrt{\mu_{max}^2 + \alpha^2 I^2}}, \quad (6)$$

where μ_0 , T , I , and α are the phytoplankton growth rate at 0°C, temperature, photosynthetically active radiation, and initial slope, respectively. I decreases exponentially with depth in the water column (z), where:

$$I(z) = I_s \cdot PARfrac \cdot \exp \left\{ -z \left(K_w + K_{chl} \int_z^0 Chl(\zeta) d\zeta \right) \right\}, \quad (7)$$

where I_s , $PARfrac$, K_{chl} , and $Chl(\zeta)$ are the shortwave radiation flux, fraction of light, light attenuation coefficient for chlorophyll- a , and chlorophyll- a concentration at a depth of ζ m, respectively. L_{nitri} is calculated as follows:

$$L_{nitri} = n_{max} \left(1 - \max \left[0, \frac{I - I_0}{k_I + I - I_0} \right] \right), \quad (8)$$

where n_{\max} , k_I , and I_0 are the maximum rate of nitrification, half-saturation for light inhibition, and inhibition threshold, respectively.

MODEL VALIDATION

To validate model performance, simulated temperatures, salinities, and NO_3^- concentrations were compared with observational data in February and August. For comparison, climatological mean data were produced from bi-monthly observation data in the southeastern YS region for the period 2006–2019. **Figures 4–6** show horizontal distributions of temperature, salinity, and NO_3^- , respectively, for the climatological observations and model results at the surface and at a depth of 50 m in February and August.

In February, the horizontal distribution at the surface showed the same pattern as at a depth of 50 m due to strong vertical mixing. A warm, saline, and low NO_3^- tongue was present in the eastern entrance of the YS, which was properly represented by the model. The concentration of NO_3^- was high in the eastern YS.

In August, the surface temperature was mostly higher than 26°C and relatively low along the western coast of the Korean Peninsula due to tidal mixing (Sun and Cho, 2010). The YSBCW was colder than 10°C in the central YS at 50-m depth. A low salinity patch ($<31 \text{ g kg}^{-1}$) appeared near Jeju Island, particularly in the western region of the island because of dilution by water from the Changjiang River. The surface NO_3^- concentration was low due to primary production but high in the western region of Jeju Island with lower-salinity waters, which was somewhat overestimated in the model. At a depth of 50 m, the NO_3^- concentration was high but relatively low in the Kuroshio Current waters, which lay east of Jeju Island. Overall, the seasonal patterns of temperature, salinity, and NO_3^- were well simulated in the coupled model.

The seasonal distributions of simulated DIN concentration were also compared in the western and central YS with the distributions presented in Wei et al. (2016; **Supplementary Figure 1**). We estimated DIN as the sum of NO_3^- and NH_4^+ and compared it with the observed DIN distributions. Surface DIN concentration is high in the central YS in winter. It decreases in summer except for high values in the mouth of the Changjiang River. The concentration increases in fall again. At the bottom layer, the DIN concentration is minimal in spring due to bloom and maximal in fall due to remineralization. The DIN concentration is normally high in the central YS where the YSBCW is located.

Due to massive fishery activities and extreme weather conditions in the YS, it is difficult to obtain long-term current data by moorings. Instead of current, surface temperatures obtained from the Advanced Very High Resolution Radiometer (AVHRR) satellite data were compared with those from model results averaged from 2006 to 2019, because horizontal distributions of surface temperature mainly depend on currents. The spring, summer, fall, and winter seasons were defined as March to May, June to August, September to November, and December to February, respectively. The distributions from the

model results presented an intrusion of warm water by the YSWC during winter and a tidal front along the Korean coast during summer and fall, indicating that the advection and mixing by currents in the YS were simulated properly with the satellite data (**Figure 7**).

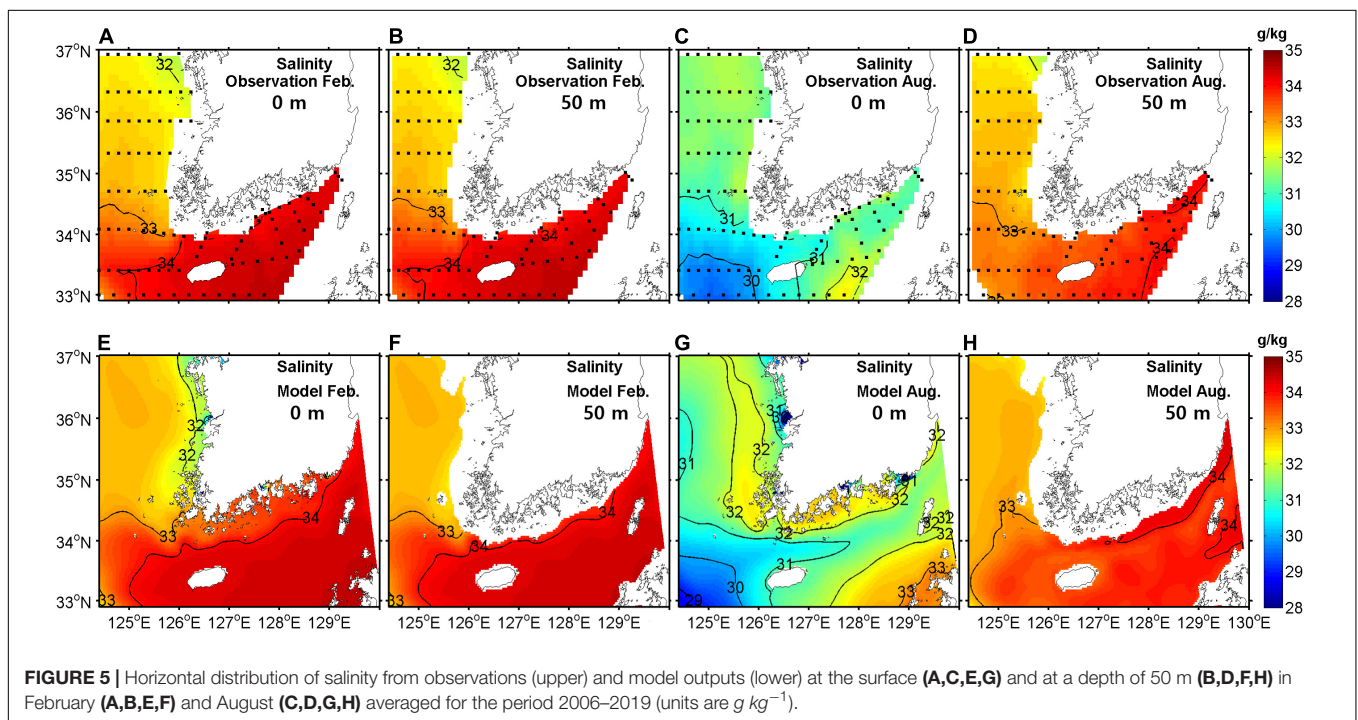
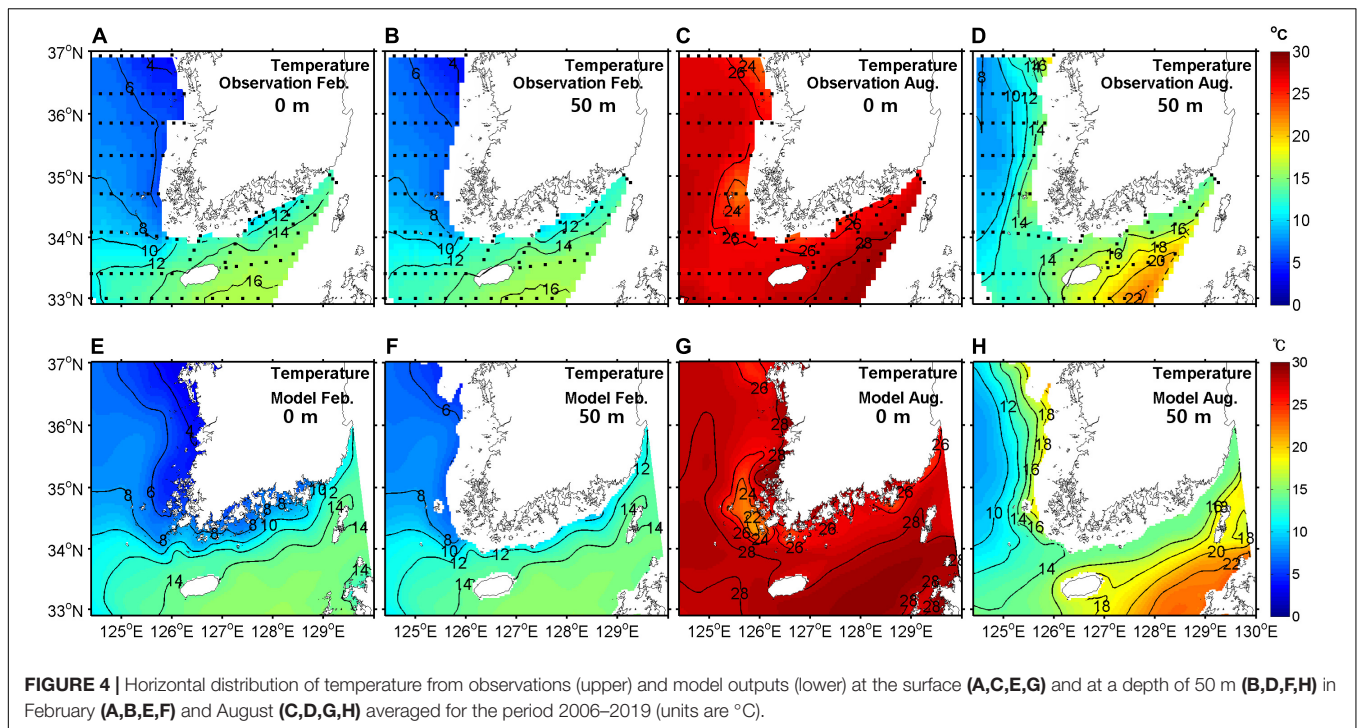
For the comparison of chlorophyll-*a* distributions, only the data in the central region of the YS ($121.5\text{--}125.5^\circ\text{E}$, $34.5\text{--}39.5^\circ\text{N}$) were selected because the chlorophyll-*a* concentration derived from satellite data was highly overestimated due to the resuspension of sediments in the coastal region of the YS and Bohai Sea (BS) (Yamaguchi et al., 2012; Shi et al., 2017). The model results were compared with the spatially averaged chlorophyll-*a* concentrations derived from MODIS-aqua for the corresponding period (**Figure 8**). Tan and Shi (2012) reported spring and fall blooms based on seasonal primary production patterns in the YS. Chlorophyll-*a* concentrations observed by satellite in winter were higher than those in fall. The high chlorophyll-*a* in winter from the satellite data might result from particle resuspension by active vertical mixing driven by strong winds in winter (Kiyomoto et al., 2001; Siswanto et al., 2011; Yamaguchi et al., 2012). Low planktonic biomass from *in situ* observations in winter supports this interpretation (Fu et al., 2009; Siswanto et al., 2011).

Overall, the Taylor diagram in **Figure 9** objectively presents the model performance for temperature, salinity, NO_3^- , and chlorophyll-*a*. The abnormal chlorophyll-*a* concentration in winter derived from the satellite data was excluded when estimating correlation, root mean square, and standard deviation. All variables except for those at a 50-m depth were close to the observation point denoted by a black star in the *x*-axis and had strong correlations higher than 0.7, suggesting that the model results nearly corresponded to the observations. The correlation coefficients and normalized standard deviations for salinity and NO_3^- at a depth of 50 m were relatively lower than other variables but the *p*-values for those variables were below 0.05, indicating significant correlations. Using various analyses of the coupled model and observation data, simulated seasonal cycles of temperature, salinity, NO_3^- , and chlorophyll-*a* by the coupled model were quantitatively evaluated and were consistent with the observations.

RESULTS AND DISCUSSION

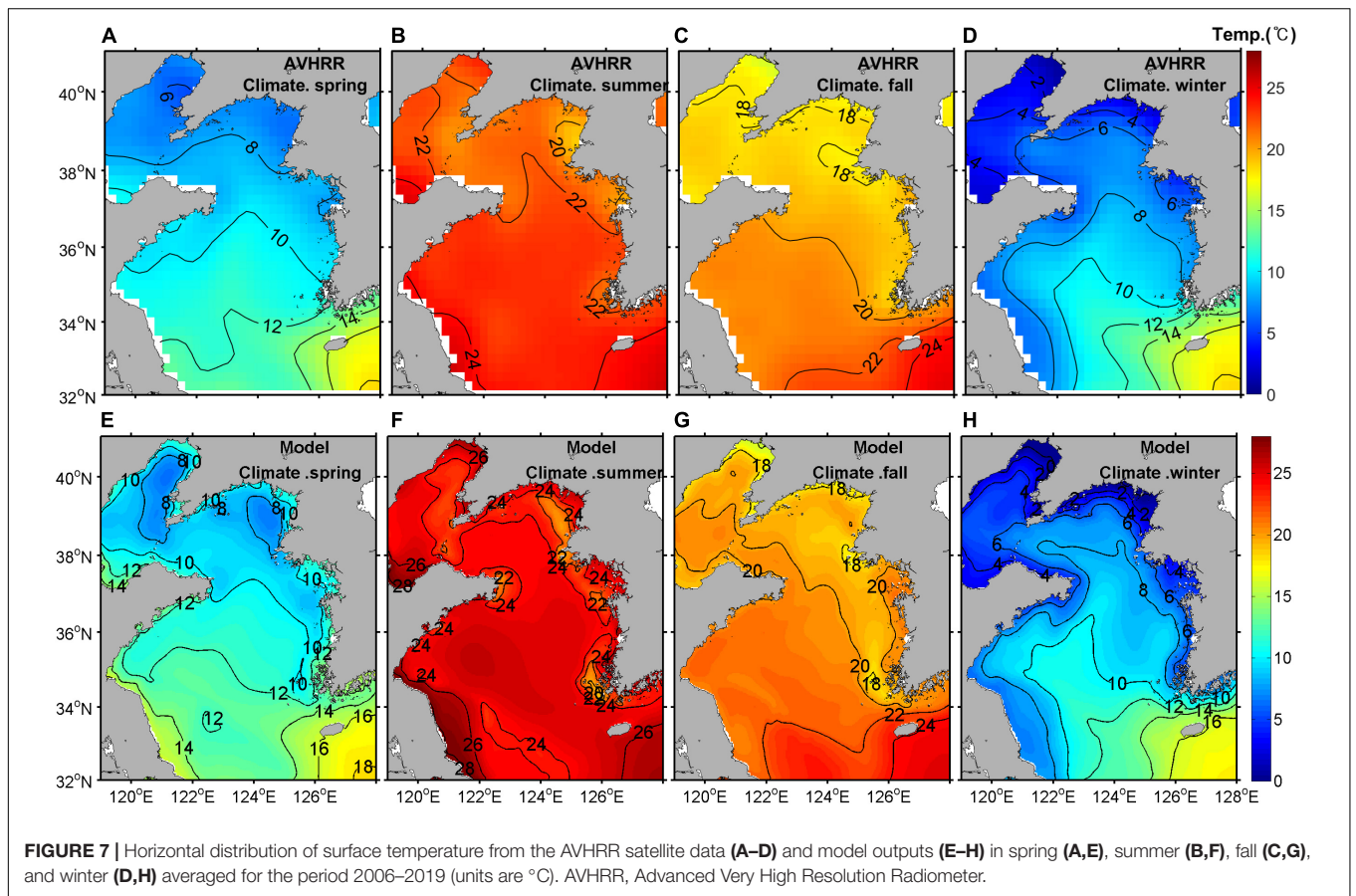
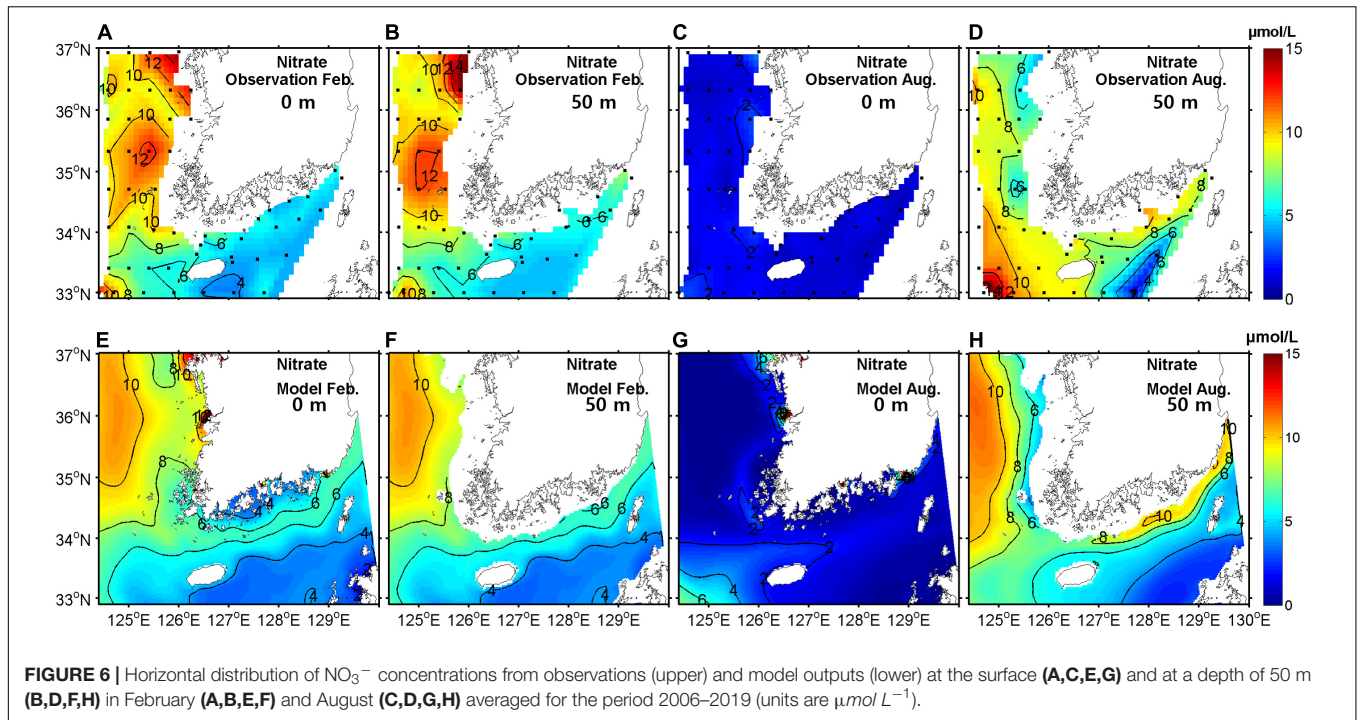
Subdivision of the Yellow Sea Based on Nitrate Flux Along the Southern Boundary and the Dominant Currents

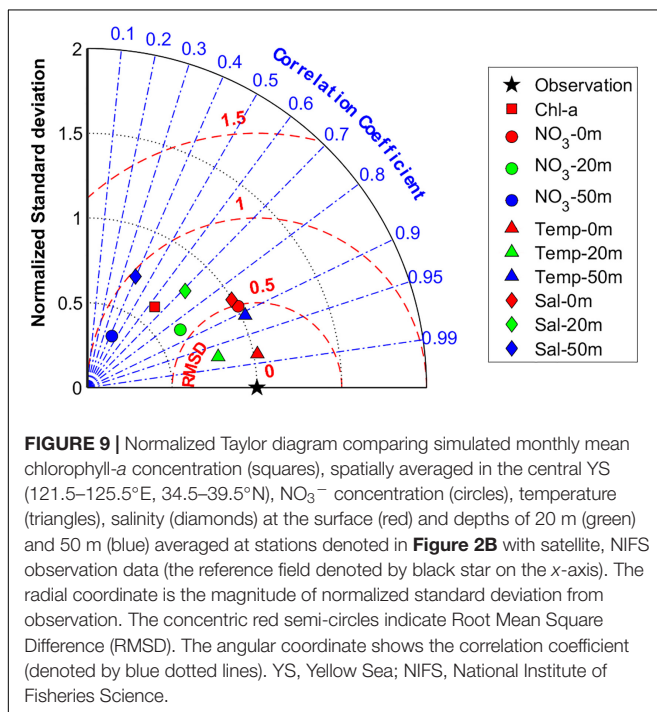
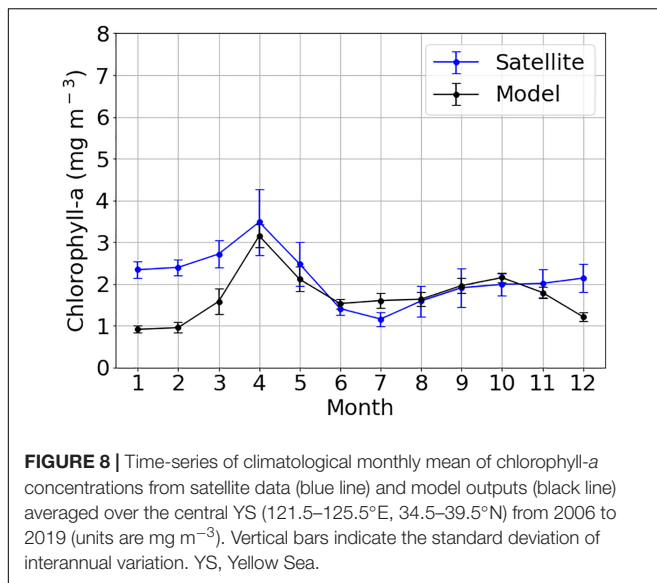
Vertical sections of NO_3^- concentrations, meridional velocity, and NO_3^- flux along the southern boundary (34.5°N) of the YS in January and July are shown in **Figure 10**. In winter, the main advective NO_3^- influxes resulted from the YSWC in the trough of the YS and SCC along the Chinese coast (**Figure 10E**). Advective outfluxes occurred with the KCC along the Korean coast and the southward surface current in the trough region (Tak et al., 2016). The YSCC located between the YSWC and the



SCC also contributed to the NO_3^- outflux, although its overall contribution was relatively small (Hwang et al., 2014). In summer, influx of NO_3^- into the YS occurred along the Chinese coast via the SCC and via a northward current on the eastern side of the trough in the subsurface layer (Figure 10F). The outflux of NO_3^- was mainly driven by the southward movement of the YSWC in the subsurface layer of the trough (Yang et al., 2014).

The southern boundary section can be divided into three areas based on the features of NO_3^- flux. In the western area of the section (119.5–121.6°E), NO_3^- was transported into the YS via the SCC all year. In the central area of the section (121.6–125.2°E), the influx occurred via the YSWC in winter and the outflux occurred via the southward movement of the YSWC in summer. In the eastern area





of the section (125.2–126.5°E), the outflux occurred via the KCC in winter.

Figure 11 shows seasonal mean horizontal velocity distributions at the surface and in the subsurface layers. Considering the surface Ekman layer depth, the surface and subsurface layers were averaged from the surface to a depth of 30 m and from 30 m to the bottom, respectively. The horizontal velocity distributions showed two representative circulation patterns, namely spring-winter and summer-fall patterns (Yanagi and Takahashi, 1993; Hwang et al., 2014). In summer and fall, a strong cyclonic circulation appeared on the surface layer with a southward current in the central YS. In spring and

winter, a southward current occurred at the surface layer in the central and eastern YS due to the strong northwesterly winter monsoon, and the northward YSWC occurred in the central YS in the subsurface layer. Anticyclonic circulation appeared in the subsurface layer. In the BS, anticyclonic circulation persisted for all seasons but was weaker than in the YS. The complex system of circulation suggests that the YS should be subdivided to adequately assess the seasonal and spatial variations in NO_3^- flux.

Considering these currents, we subdivided the YS into the northern YS (nYS), southeastern YS (seYS), southcentral YS (scYS), and southwestern YS (swYS) as shown in **Figure 12A**. The BS was designated as a separate subregion. We further divided the boundaries between swYS and scYS, and between scYS and seYS, into northern (solid line) and southern (dashed line) boundaries. The boundary between nYS and scYS was divided into eastern (solid line) and western (dashed line) boundaries.

Advective Nitrate Flux Across Subregion Boundaries

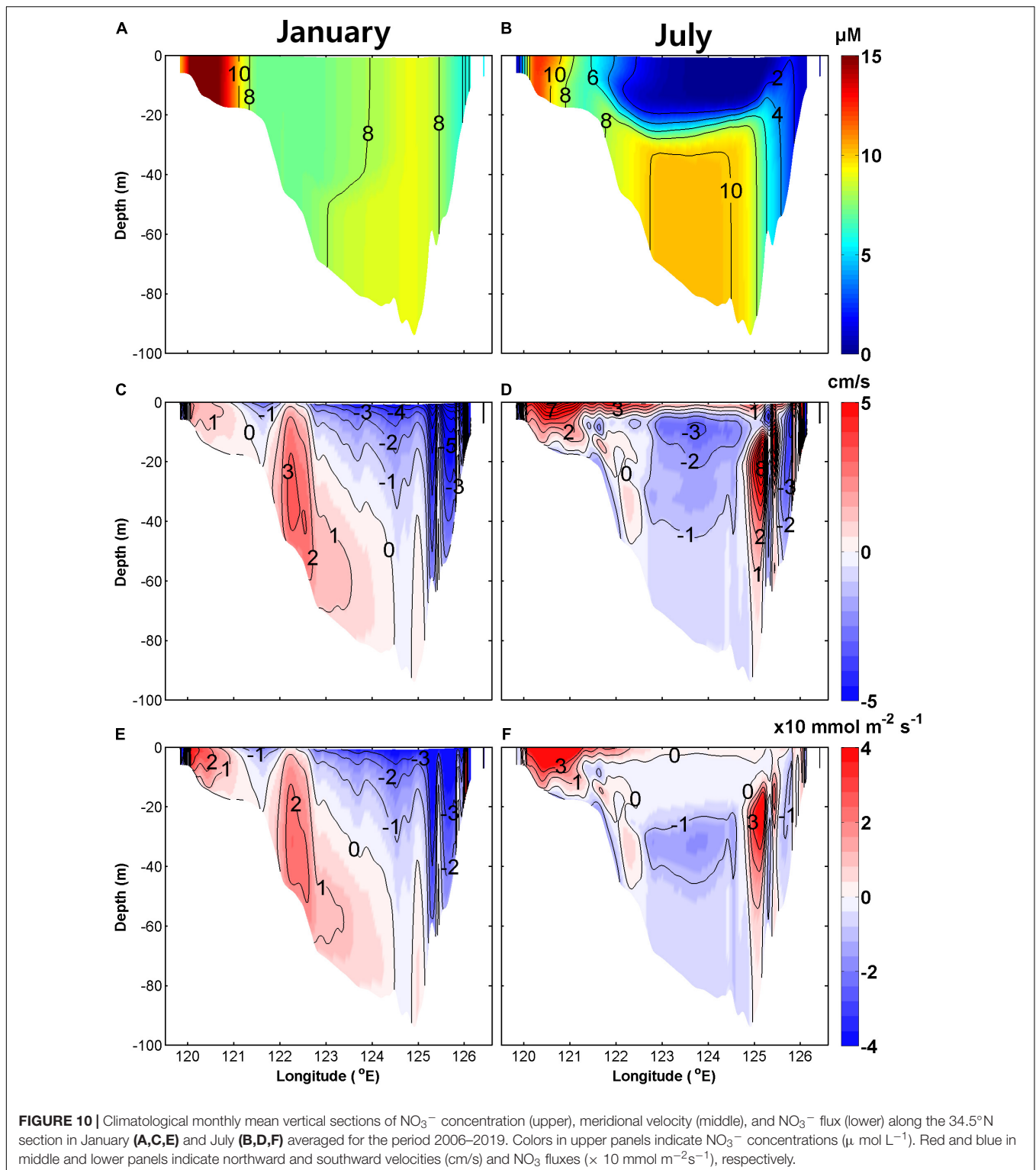
The monthly mean net advective NO_3^- fluxes by currents among subregions were calculated. The BS supplied NO_3^- to the nYS year round except in summer (**Figure 12B**). The net advective fluxes across boundaries in the YS exhibited strong seasonal variation. In winter, northward and southward fluxes occurred across the western and eastern boundaries between the nYS and scYS, respectively (**Figure 12C**). Net fluxes across the meridional boundaries dividing the swYS, scYS, and seYS similarly showed westward and eastward fluxes across the southern and northern boundaries, respectively (**Figures 12D,E**). Net fluxes in summer occurred in the opposite directions to those in winter in accordance with the circulation direction.

The net advective fluxes across the southern boundary of the YS represent fluxes between the YS and the ECS (**Figure 12F**). Influx to the swYS (red dashed line) via the SCC along the Chinese coast played a major role in the net influx from the ECS. The net influx to the scYS (red solid line) via the YSWC during winter was relatively small. The mean influx of NO_3^- via the YSWC was $1.4 \cdot 10^3 \text{ mol s}^{-1}$ during winter but was almost offset by the southward current in the surface layer. Net outfluxes to the ECS occurred from the scYS in summer due to the southward movement of the YSBCW and from the seYS in winter via the KCC along the Korean coast (red dotted line in **Figure 12A**).

Nitrate Budgets in the Subregions

Monthly mean changes in NO_3^- concentration driven by current advection, biological processes, and riverine input were calculated for each subregion (**Figure 13**) and are summarized in **Supplementary Table 1**. In the BS, advective influx of NO_3^- was much smaller than inputs from biological processes (**Figure 13A**). The advective influx changed little year round, whereas nitrification was maximal in fall and uptake by phytoplankton occurred predominantly in spring.

In the nYS, advective influx of NO_3^- was comparable with the change driven by biological processes in fall and winter, but was much smaller in spring and summer when uptake by



phytoplankton was high (**Figure 13B**). The uptake consumed NO_3^- during the spring and fall blooms and nitrification supplied NO_3^- in summer because of stratification of the water column and active remineralization after the spring bloom. Total advective influx of NO_3^- was $14.0 \times 10^3 \text{ mol s}^{-1}$ and the outflux

was $15.2 \times 10^3 \text{ mol s}^{-1}$. The supply by nitrification and uptake was 19.3×10^3 and $22.8 \times 10^3 \text{ mol s}^{-1}$, respectively. NO_3^- flux from the Yalu River was $3.2 \times 10^3 \text{ mol s}^{-1}$.

In the swYS, advective influx of NO_3^- was nearly comparable to the supply by nitrification year round (**Figure 13C**). The

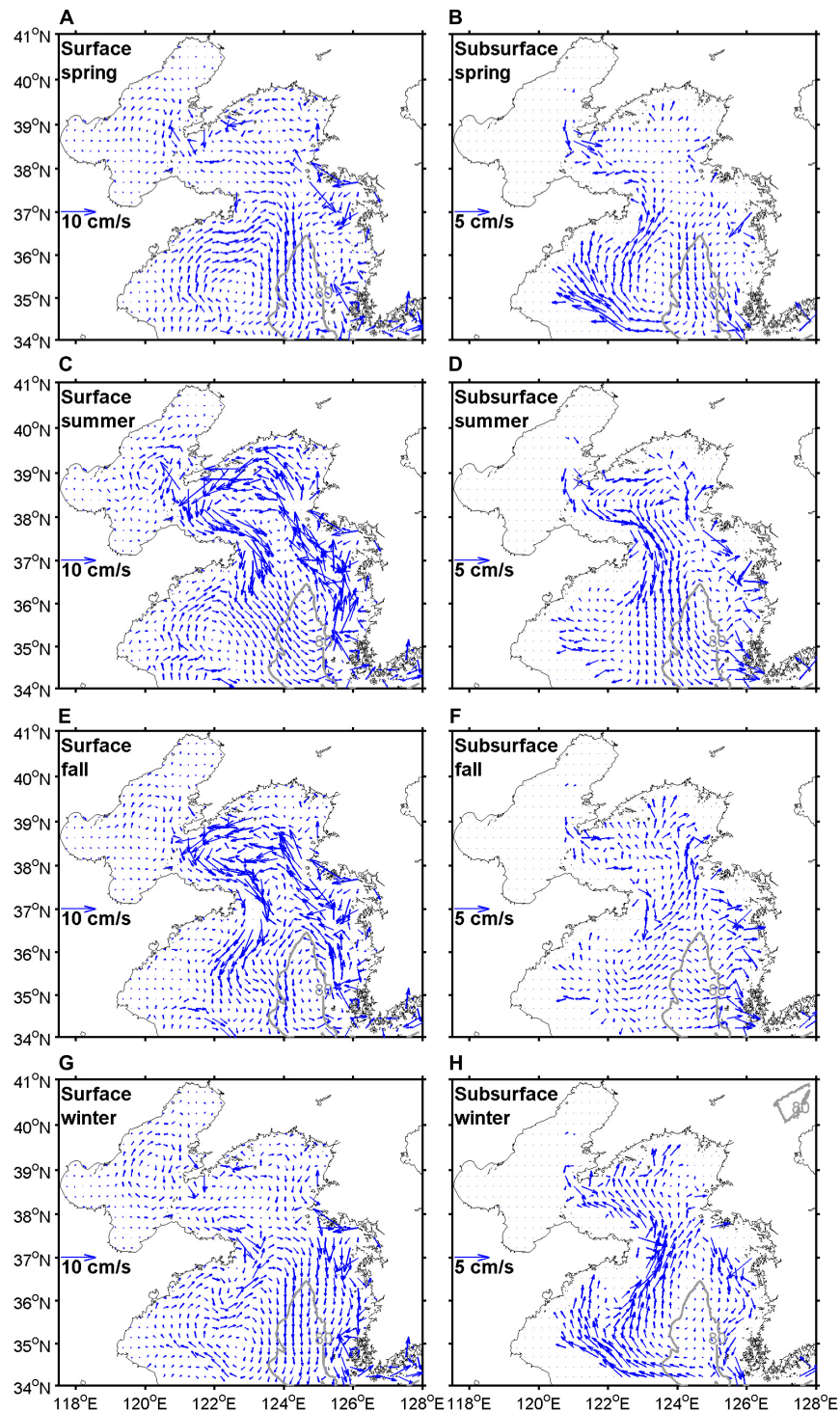
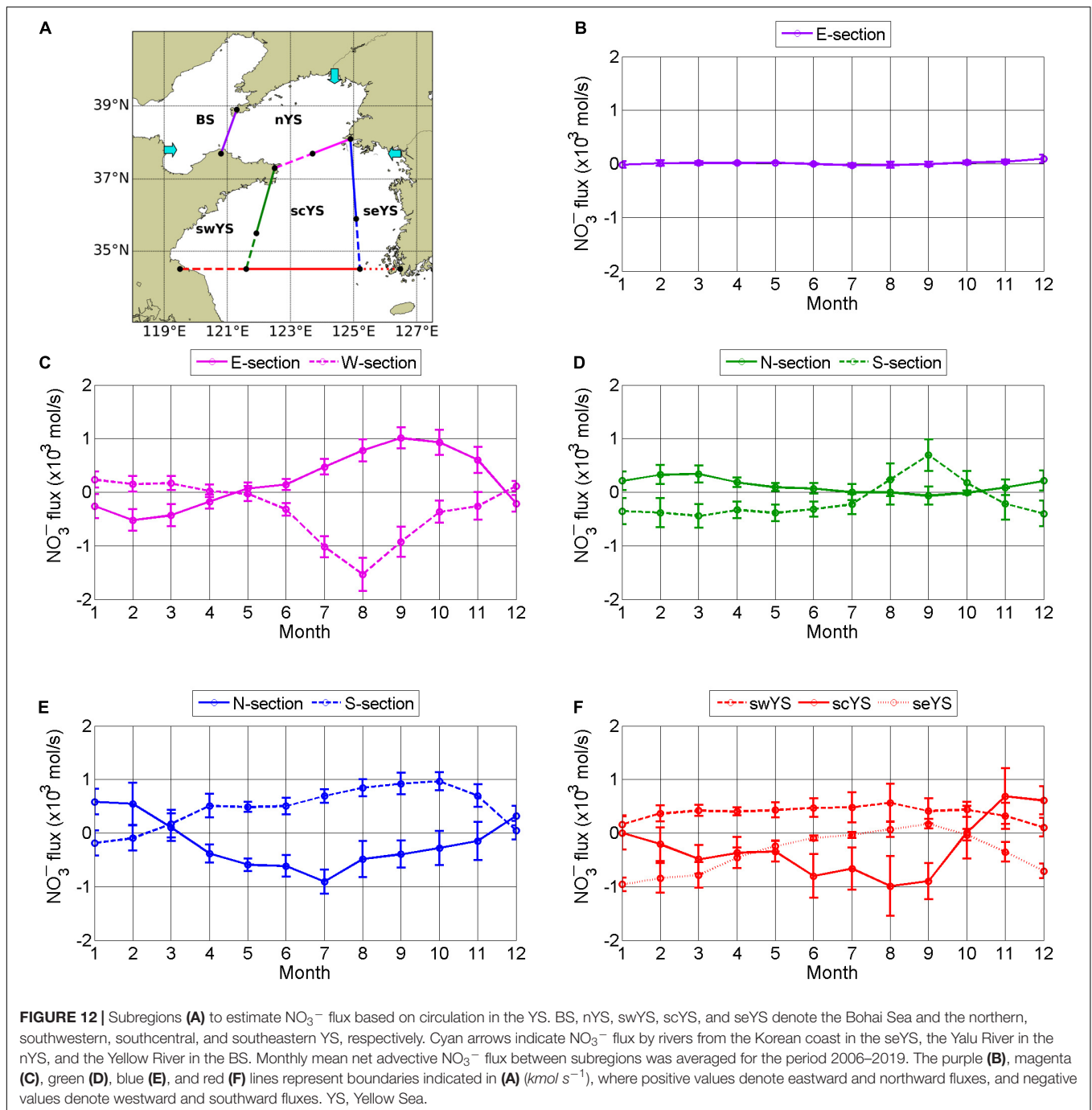


FIGURE 11 | Horizontal velocity distributions at the surface (A–D) and subsurface (E–H) layers during spring (A,E), summer (B,F), fall (C,G), and winter (D,H) averaged for the period 2006–2019. The surface and subsurface layers are averaged from the surface to 30 m depth and from 30 m depth to the bottom, respectively.

advective outflux was lower than the uptake. The supply and consumption of NO_3^- by biological processes in the swYS were similar to those in the BS. Total advective influx and

outflux were 10.8×10^3 and $5.7 \times 10^3 \text{ mol s}^{-1}$, respectively, and supply by nitrification and uptake were 12.0×10^3 and $14.8 \times 10^3 \text{ mol s}^{-1}$, respectively.

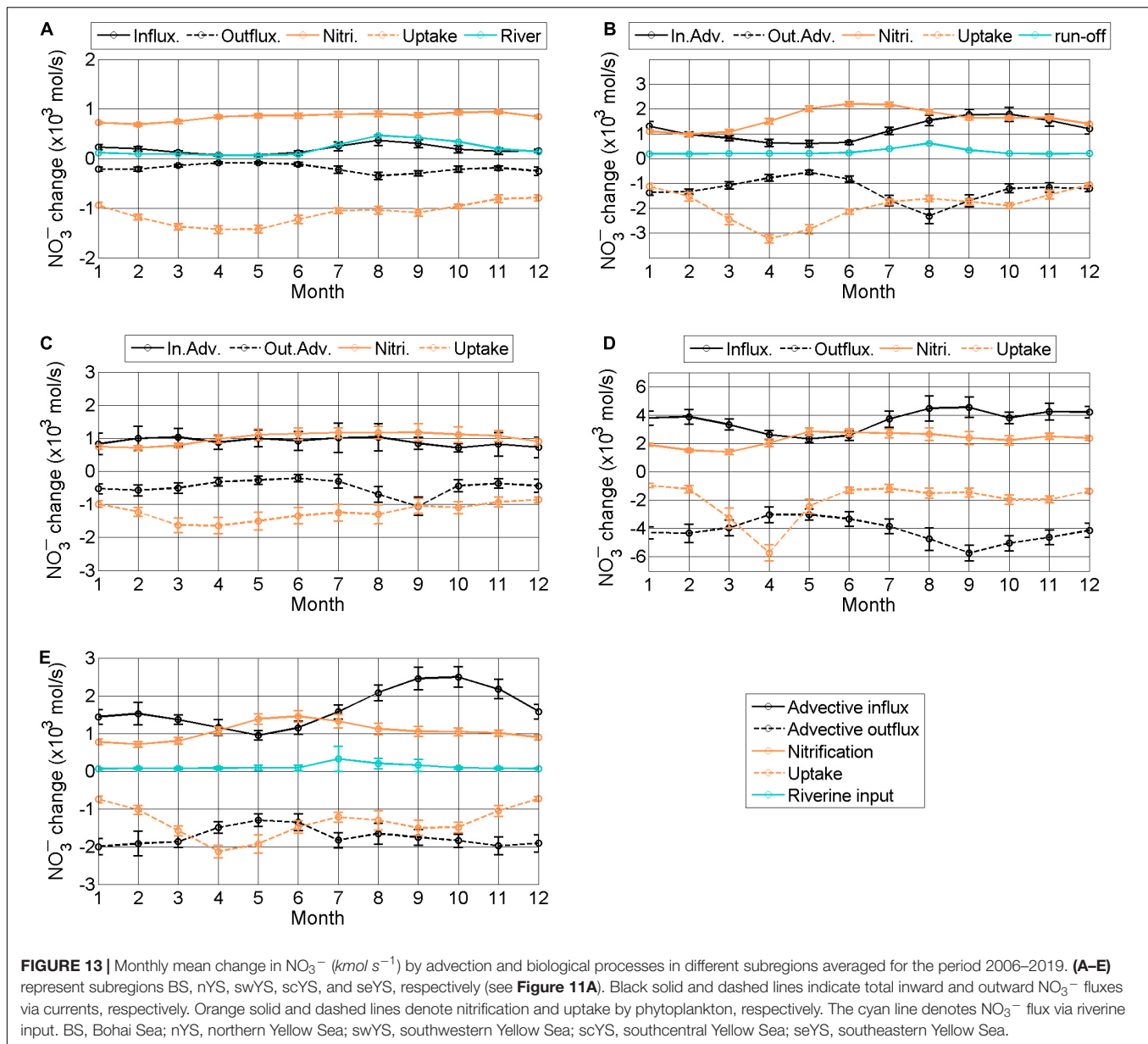


In the scYS, advective influx of NO_3^- was two times higher than the supply by nitrification except from April to June (Figure 13D). The advective outflux was larger than biological consumption all year except in April. Total advective influx and outflux were 44.5×10^3 and $50.4 \times 10^3 \text{ mol s}^{-1}$, respectively, and the changes from nitrification and uptake yield were 27.7×10^3 and $24.3 \times 10^3 \text{ mol s}^{-1}$, respectively.

NO_3^- in the seYS was also primarily supplied by advection, which was especially strong in fall (Figure 13E). The seasonal variation in nitrification and uptake in the seYS had a similar

pattern as those in subregions nYS and scYS. Total advective influx and outflux were 20.0×10^3 and $20.9 \times 10^3 \text{ mol s}^{-1}$, respectively, and the changes from nitrification and uptake yield were 12.7×10^3 and $16.2 \times 10^3 \text{ mol s}^{-1}$, respectively. NO_3^- flux from rivers along the Korean coast was $1.4 \times 10^3 \text{ mol s}^{-1}$.

The model results clearly demonstrated that advection played a major role in the total NO_3^- budget in the central and eastern regions of the YS and that biological processes were a major factor regulating the budget in the western and northern regions of the YS and the BS. However,



the relative importance of these processes varied between seasons. Notably, changes in NO_3^- driven both by currents and biological processes were essential for understanding the NO_3^- budgets and ultimately, the ecosystem in the YS and BS.

Seasonal and Spatial Variations in Nitrate Budgets

The schematic diagrams for net NO_3^- fluxes by physical and biological processes indicate the dominant factors controlling seasonal NO_3^- fluxes in each subregion (Figure 14). Net advective NO_3^- flux was anticyclonic in spring and winter but cyclonic in summer and fall following the dominant seasonal circulation patterns.

Net advective influx from the ECS occurred via the SCC along the Chinese coast in the swYS year round. Previous studies suggested that 0.6×10^3 to $6.1 \times 10^3 \text{ mol s}^{-1}$ of DIN is transported into the swYS from the Changjiang River (Li et al., 2014, 2015), corresponding to $1.2 \times 10^3 \text{ mol s}^{-1}$ of NO_3^- from the model results. Additionally, the model results indicate that influx from the scYS into the swYS during winter and spring is also a substantial source (Figure 14). The influx of NO_3^- via the YSWC in the lower layer across the southern boundary of the scYS in winter was considerable but net flux across the boundary was very low because this flux was almost offset by the southward current-driven flux at the surface (Figure 14D). Although previous studies proposed that the YSWC could supply high NO_3^- water to the YS, the horizontal distributions from observed data (Figures 4–6) showed that a

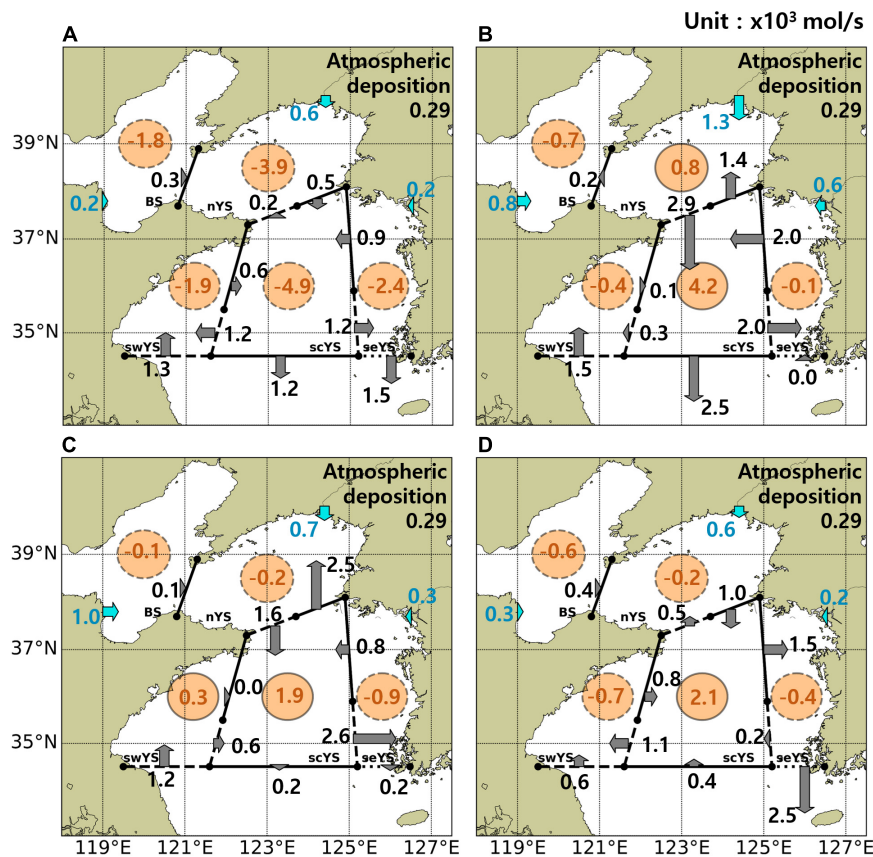


FIGURE 14 | NO_3^- (kmol s^{-1}) budgets in subregions of the YS in spring (A), summer (B), fall (C), and winter (D) averaged for the period 2006–2019. Gray arrows indicate the net advective fluxes between subregions. Cyan arrows denote the net fluxes from rivers. Orange circles denote supply (solid circle) or consumption (dashed circle) by biological processes. YS, Yellow Sea.

warm and saline water mass intrusion with poor NO_3^- (Jin et al., 2013; Zhou et al., 2013; Liu et al., 2015a). Moreover, the net advective influx into the scYS during winter, when the YSWC is the strongest, was insignificant. This indicates that nitrification is a more crucial source of NO_3^- in the scYS. Net advective outfluxes from the scYS occurred via the southward movement of the YSBCW in summer (Figure 14B) and from the seYS via the KCC in winter (Figure 14D). Although the advective outflux to the ECS is approximately one order of magnitude lower than other fluxes to the ECS, such as the Taiwan Warm Current, Changjiang River, and Kuroshio Current (Kim S. K. et al., 2013), it is likely to affect the southern coast of Korea because the KCC and YSBCW can flow into the southern coastal sea of Korea (Cho and Kim, 1994; Cho et al., 1995; Bae et al., 2014; Um et al., 2018). Thus, understanding the assessment of and variability in the advective outflux from the YS would be important to investigate the ecosystem over the Korean coast. Influxes of NO_3^- from the Yalu, Han, and Geum Rivers, and the atmospheric deposition were smaller than the fluxes via currents in the subregions; however, influx from the Yellow River was comparable to the advective flux in the BS where biological processes dominated the NO_3^- budget.

The consumption by phytoplankton was greater than the supply by nitrification in all subregions during spring (Figure 14A). Net consumption by biological processes continued in summer in shallow coastal regions, such as the seYS, swYS, and BS (Figure 14B), where active tidal mixing provides favorable conditions for phytoplankton by supplying nitrate to the euphotic layer (Sun and Cho, 2010). Biological uptake was lower than nitrification in offshore regions (i.e., scYS and nYS) with strong stratification in summer, which inhibited the supply of NO_3^- from the lower layer to the surface and, instead, provided a suitable environment for nitrification in the lower layer. Moreover, the advection in summer even exports NO_3^- to the ECS so that nitrification mainly results in an increase in DIN in the bottom layer of the YS, as indicated by our model results and previous observations (Supplementary Figure 1; Chen, 2009; Jin et al., 2013; Wei et al., 2016). The net supply by biological processes was the highest in the scYS during summer due to active organic matter decomposition and nitrification in the YSBCW, and the supply continued until winter. Wu et al. (2019) proposed that remineralization and nitrification are key processes to supply NO_3^- in the YSBCW. The model results also show the importance of nitrification as the source of NO_3^- and its seasonal contribution to the budgets.

Limitations of the Model

Seasonal contributions of NO_3^- budgets to biological and physical fluxes in the YS were estimated using a physical-biogeochemical numerical model. However, deficiencies in observation data and some parameterization should be improved to provide more precise assessments. In this study, organic matter was remineralized as soon as it reached the bottom layer but it is gradually decomposed depending on complicated physical and biogeochemical conditions, such as oxygen content, temperature, bacterial activity, and turbulence, in the real ocean (Glud, 2008). These conditions can vary tempo-spatially with external factors; thus, periodic and wide-ranging investigations are needed to estimate precise NO_3^- budgets.

Seasonal NO_3^- budgets from the numerical model indicated that the atmospheric flux was much lower than other sources although the flux did not consider tempo-spatial variation. However, recent studies revealed that the contribution of atmospheric deposition to NO_3^- budgets in the YS continues to increase due to anthropogenic activity (Zhang et al., 2007; Luo et al., 2018; Wang et al., 2020). Thus, the impact of a recent increase in the atmospheric deposition on budgets in the YS will be investigated through regular observation and an atmospheric-ocean coupled model.

Previous studies indicated a positive trend of NO_3^- in the southwestern YS from 2005 to 2012 but a negative trend in the southeastern YS from 2000 to 2014 (NFRDI, 2014; Li et al., 2015). Although our model results presented the same trend direction in each region, because most of the boundary conditions did not consider the inter-annual and long-term variability in our model, values of the trends from the model were different from observed data and it was difficult to determine the real causes of increased or decreased budgets. To reveal the causes of the long-term variability in nutrients due to climate change, cooperation with countries near the YS and regular investigations of the nutrient concentrations of rivers and the open ocean for the lateral boundary conditions are essential.

SUMMARY AND CONCLUSION

A physical-biogeochemical coupled model experiment was performed to assess the seasonal and spatial variations in NO_3^- budgets in the YS. By comparison with observation data, the model demonstrated reasonable simulation of the seasonal variations in temperature, salinity, chlorophyll-*a*, and NO_3^- . The model enabled us to quantitatively address the relative contribution of advective transport and biological processes in NO_3^- budgets in each subregion of the YS. Advective NO_3^- flux via currents was dominant in the central and eastern regions of the YS whereas biological flux was dominant in the western and northern regions of the YS. NO_3^- was transported cyclonically in summer and fall and anticyclonically in spring and winter following the dominant current patterns. Riverine input of NO_3^- was minor compared to the contributions of

advective fluxes and biological consumption/production. The model results suggested that the SCC along the Chinese coast was a major source of NO_3^- from the ECS year round. Influx via the YSWC was offset by outflux via a southward surface current driven by the northerly wind in winter. The southward movement of the YSBCW in summer and the KCC in winter mainly drove NO_3^- export to the ECS. The influence of biological processes on NO_3^- budgets was negative in spring due to algal blooms and positive in summer due to active decomposition of organic matter and consequent nitrification. Nitrification was the largest net supplier of NO_3^- in the scYS, where the YSBCW was present.

Overall, our analyses provide initial quantitative assessment of each process including advective transport by currents, biological processes, and riverine inputs in NO_3^- budgets in the YS. Temporal and spatial variations in atmospheric deposition, sediments, and groundwater may also be important in the seasonal variation in NO_3^- ; incorporation of these additional factors in future studies will further refine the model. Our study demonstrates the usefulness of the coupled model in assessing budgets of biogeochemically important parameters. This type of modeling can be adopted to address carbon transport off the shelf, for example, out of the YS in the future. In addition, causes of the annual and decadal variability in the biogeochemical processes in the YS should be investigated using the coupled model through more sophisticated model configurations.

DATA AVAILABILITY STATEMENT

The original contributions presented in the study are included in the article/**Supplementary Material**, further inquiries can be directed to the corresponding author/s.

AUTHOR CONTRIBUTIONS

Y-JT and Y-KC: conceptualization. Y-JT and Y-YK: methodology. Y-JT: writing draft and visualization. Y-KC and JH: review and editing. Y-KC: supervision. All authors contributed to the article and approved the submitted version.

FUNDING

This study was supported by the project “Deep Water Circulation and Material Cycling in the East Sea (20160400)” funded by the Ministry of Oceans and Fisheries (MOF), Republic of Korea.

SUPPLEMENTARY MATERIAL

The Supplementary Material for this article can be found online at: <https://www.frontiersin.org/articles/10.3389/fmars.2021.785377/full#supplementary-material>

REFERENCES

- Bach, L. T., Riebesell, U., Sett, S., Febiri, S., Rzepka, P., and Schulz, K. G. (2012). An approach for particle sinking velocity measurements in the 3–400 μm size range and considerations on the effect of temperature on sinking rates. *Mar. Biol.* 159, 1853–1864. doi: 10.1007/s00227-012-1945-2
- Bae, S. H., Kim, D. C., Lee, G. S., Kim, G. Y., Kim, S. P., Seo, Y. K., et al. (2014). Physical and acoustic properties of inner shelf sediments in the South Sea, Korea. *Quat. Int.* 344, 125–142. doi: 10.1016/j.quaint.2014.03.058
- Bashkin, V. N., Park, S. U., Choi, M. S., and Lee, C. B. (2002). “Nitrogen budgets for the Republic of Korea and the Yellow Sea region,” in *The Nitrogen Cycle at Regional to Global Scales*, eds E. W. Boyer and R. W. Howarth (Dordrecht: Springer), 387–403. doi: 10.1007/978-94-017-3405-9_12
- Beardsley, R. C., Limeburner, R., Kim, K., and Candela, J. (1992). Lagrangian flow observations in the East China, Yellow and Japan seas. *La Mer* 30, 297–314.
- Castillo-Ramírez, A., Santamaría-del-Ángel, E., González-Silvera, A., Frouin, R., Sebastia-Frasquet, M.-T., Tan, J., et al. (2020). A new algorithm to estimate diffuse attenuation coefficient from Secchi disk depth. *J. Mar. Sci. Eng.* 8:558. doi: 10.3390/jmse8080558
- Chen, C. T. A. (2009). Chemical and physical fronts in the Bohai, Yellow and East China seas. *J. Mar. Syst.* 78, 394–410. doi: 10.1016/j.jmarsys.2008.11.016
- Chengkui, Z. (1984). Phycological research in the development of the Chinese seaweed industry. *Hydrobiologia* 116, 7–18. doi: 10.1007/BF00027633
- Cho, Y.-K., and Kim, K. (1994). Characteristics and origin of the cold water in the South Sea of Korea in summer. *J. Korean Soc. Oceanogr.* 29, 414–421.
- Cho, Y.-K., Kim, K., and Rho, H.-K. (1995). Salinity decrease and the transport in the South Sea of Korea in summer. *J. Ocean Eng. Technol.* 7, 126–134.
- Copernicus Climate Change Service (2017). *Data from: ERA5: Fifth Generation of ECMWF Atmospheric Reanalyses of the Global Climate*. European Union (EU). Available online at: <https://cds.climate.copernicus.eu/cdsapp#!/home> (accessed April 1, 2021).
- Dai, Z., Du, J., Zhang, X., Su, N., and Li, J. (2011). Variation of riverine material loads and environmental consequences on the Changjiang (Yangtze) Estuary in recent decades (1955–2008). *Environ. Sci. Technol.* 45, 223–227. doi: 10.1021/es103026a
- Egbert, G. D., and Erofeeva, S. Y. (2002). Efficient inverse modeling of barotropic ocean tides. *J. Atmos. Oceanic Technol.* 19, 183–204.
- Fairall, C. W., Bradley, E. F., Rogers, D. P., Edson, J. B., and Young, G. S. (1996). Bulk parameterization of air-sea fluxes for tropical ocean-global atmosphere coupled-ocean atmosphere response experiment. *J. Geophys. Res. Ocean.* 101, 3747–3764. doi: 10.1029/95JC03205
- Fasham, M. J. R., Ducklow, H. W., and McKelvie, S. M. (1990). A nitrogen-based model of plankton dynamics in the oceanic mixed layer. *J. Mar. Res.* 48, 591–639. doi: 10.1357/002224090784984678
- Fennel, K., Wilkin, J., Levin, J., Moisan, J., O’Reilly, J., and Haidvogel, D. (2006). Nitrogen cycling in the middle Atlantic bight: results from a three-dimensional model and implications for the North Atlantic nitrogen budget. *Glob. Biogeochem. Cycles* 20:GB3007. doi: 10.1029/2005GB002456
- Fu, M., Sun, P., Wang, Z., Wei, Q., Qu, P., Zhang, X., et al. (2018). Structure, characteristics and possible formation mechanisms of the subsurface chlorophyll maximum in the Yellow Sea Cold Water Mass. *Cont. Shelf Res.* 165, 93–105. doi: 10.1016/j.csr.2018.07.007
- Fu, M., Wang, Z., Li, Y., Li, R., Sun, P., Wei, X., et al. (2009). Phytoplankton biomass size structure and its regulation in the Southern Yellow Sea (China): seasonal variability. *Cont. Shelf Res.* 29, 2178–2194. doi: 10.1016/j.csr.2009.08.010
- Gan, J., Lu, Z., Cheung, A., Dai, M., Liang, L., Harrison, P. J., et al. (2014). Assessing ecosystem response to phosphorus and nitrogen limitation in the Pearl River plume using the regional ocean modeling system (ROMS). *J. Geophys. Res. Oceans* 119, 8858–8877. doi: 10.1002/2014JC009951
- García, H. E., Locarnini, R. A., Boyer, T. P., Antonov, J. I., Baranova, O. K., Zweng, M. M., et al. (2013). *Data from: World Ocean Atlas 2013. Volume 4, Dissolved Inorganic Nutrients (Phosphate, Nitrate, Silicate)*. NOAA Atlas NESDIS 76. Silver Spring, MD: National Oceanographic Data Center, 25. doi: 10.7289/V5J67DWD
- Glud, R. N. (2008). Oxygen dynamics of marine sediments. *Mar. Biol. Res.* 4, 243–289. doi: 10.1080/17451000801888726
- Gong, Y., Yu, Z., Yao, Q., Chen, H., Mi, T., and Tan, J. (2015). Seasonal variation and sources of dissolved nutrients in the Yellow River, China. *Int. J. Environ. Res. Public Health* 12, 9603–9622. doi: 10.3390/ijerph120809603
- Gruber, N., Frenzel, H., Doney, S. C., Marchesiello, P., McWilliams, J. C., Moisan, J. R., et al. (2006). Eddy-resolving simulation of plankton ecosystem dynamics in the California current system. *Deep Sea Res. Part 1 Oceanogr. Res. Pap.* 53, 1483–1516. doi: 10.1016/j.dsr.2006.06.005
- Guo, C., Zhang, G., Sun, J., Leng, X., Xu, W., Wu, C., et al. (2020). Seasonal responses of nutrient to hydrology and biology in the southern Yellow Sea. *Cont. Shelf Res.* 206:104207. doi: 10.1016/j.csr.2020.104207
- Holmes, R. W. (1970). The Secchi disk in turbid coastal waters. *Limnol. Oceanogr.* 15, 688–694. doi: 10.4319/lo.1970.15.5.0688
- Howarth, R. W. (1988). Nutrient limitation of net primary production in marine ecosystems. *Ann. Rev. Ecol.* 19, 89–110. doi: 10.1146/annurev.es.19.110188.000513
- Hsueh, Y. (1988). Recent current observations in the eastern Yellow Sea. *J. Geophys. Res. Oceans* 93, 6875–6884. doi: 10.1029/JC093iC06p06875
- Hwang, J. H., Van, S. P., Choi, B.-J., Chang, Y. S., and Kim, Y. H. (2014). The physical processes in the Yellow Sea. *Ocean Coast. Manag.* 102, 449–457. doi: 10.1016/j.ocecoaman.2014.03.026
- Hyun, J.-H., and Kim, K.-H. (2003). Bacterial abundance and production during the unique spring phytoplankton bloom in the central Yellow Sea. *Mar. Ecol. Prog. Ser.* 252, 77–88. doi: 10.3354/meps252077
- Jang, P.-G., Lee, T. S., Kang, J.-H., and Shin, K. (2013). The influence of thermohaline fronts on chlorophyll a concentrations during spring and summer in the southeastern Yellow Sea. *Acta Ocean. Sin.* 32, 82–90. doi: 10.1007/s13131-013-0355-8
- Jin, J., Liu, S. M., Ren, J. L., Liu, C. G., Zhang, J., Zhang, G. L., et al. (2013). Nutrient dynamics and coupling with phytoplankton species composition during the spring blooms in the Yellow Sea. *Deep Sea Res. Part 2 Top. Stud. Oceanogr.* 97, 16–32. doi: 10.1016/j.dsr2.2013.05.002
- Kim, C.-S., Cho, Y.-K., Choi, B.-J., Jung, K. T., and You, S. H. (2013). Improving a prediction system for oil spills in the Yellow Sea: effect of tides on subtidal flow. *Mar. Pollut. Bull.* 68, 85–92. doi: 10.1016/j.marpolbul.2012.12.018
- Kim, J. K., Yarish, C., Hwang, E. K., Park, M., and Kim, Y. (2017). Seaweed aquaculture: cultivation technologies, challenges and its ecosystem services. *Algae* 32, 1–13. doi: 10.4490/algae.2017.32.3.3
- Kim, S. K., Chang, K. I., Kim, B., and Cho, Y. K. (2013). Contribution of ocean current to the increase in N abundance in the Northwestern Pacific marginal seas. *Geophys. Res. Lett.* 40, 143–148. doi: 10.1029/2012GL054545
- Kim, T. W., Lee, K., Najjar, R. G., Jeong, H.-D., and Jeong, H. J. (2011). Increasing N abundance in the Northwestern Pacific Ocean due to atmospheric nitrogen deposition. *Science* 334, 505–509. doi: 10.1126/science.1206583
- Kiyomoto, Y., Iseki, K., and Okamura, K. (2001). Ocean color satellite imagery and shipboard measurements of chlorophyll a and suspended particulate matter distribution in the East China Sea. *J. Oceanogr.* 57, 37–44. doi: 10.1023/A:1011170619482
- Large, W. G., McWilliams, J. C., and Doney, S. C. (1994). Oceanic vertical mixing: a review and a model with a nonlocal boundary layer parameterization. *Rev. Geophys.* 32, 363–403. doi: 10.1029/94RG01872
- Li, H.-M., Tang, H.-J., Shi, X.-Y., Zhang, C.-S., and Wang, X.-L. (2014). Increased nutrient loads from the Changjiang (Yangtze) river have led to increased harmful algal blooms. *Harmful Algae* 39, 92–101. doi: 10.1016/j.hal.2014.07.002
- Li, H.-M., Zhang, C.-S., Han, X.-R., and Shi, X.-Y. (2015). Changes in concentrations of oxygen, dissolved nitrogen, phosphate, and silicate in the southern Yellow Sea, 1980–2012: sources and seaward gradients. *Estuar. Coast. Shelf Sci.* 163, 44–55. doi: 10.1016/j.ecss.2014.12.013
- Lie, H.-J., Cho, C.-H., Lee, J.-H., Lee, S., Tang, Y., and Zou, E. (2001). Does the Yellow Sea warm current really exist as a persistent mean flow? *J. Geophys. Res. Ocean.* 106, 22199–22210. doi: 10.1029/2000JC000629
- Lim, D.-I., Kang, M.-R., Jang, P.-G., Kim, S.-Y., Jung, H.-S., Kang, Y.-S., et al. (2008). Water quality characteristics along midwestern coastal area of Korea (in Korean). *Ocean Polar Res.* 30, 379–399. doi: 10.4217/OPR.2008.30.4.379
- Lin, X., and Yang, J. (2011). An asymmetric upwind flow, Yellow Sea Warm Current: 2. Arrested topographic waves in response to the northwesterly wind. *J. Geophys. Res. Oceans* 116:C04027. doi: 10.1029/2010JC006514
- Lin, X., Yang, J., Guo, J., Zhang, Z., Yin, Y., Song, X., et al. (2011). An asymmetric upwind flow, Yellow Sea Warm Current: 1. New observations in the western Yellow Sea. *J. Geophys. Res. Oceans* 116:C04026. doi: 10.1029/2010JC006513
- Liu, D., Keesing, J. K., He, P. M., Wang, Z. L., Shi, Y. J., and Wang, Y. J. (2013). The world’s largest macroalgal bloom in the Yellow Sea, China: formation and implications. *Estuar. Coast. Shelf Sci.* 129, 2–10. doi: 10.1016/j.ecss.2013.05.021

- Liu, S., and Zhang, J. (2004). Nutrient dynamics in the macro-tidal Yalujiang Estuary. *J. Coast. Res.* 43, 147–161.
- Liu, S. M., Altabet, M. A., Zhao, L., Larkum, J., Song, G. D., Zhang, G. L., et al. (2017). Tracing nitrogen biogeochemistry during the beginning of a spring phytoplankton bloom in the yellow sea using coupled nitrate nitrogen and oxygen isotope ratios. *J. Geophys. Res. Biogeosci.* 122, 2490–2508. doi: 10.1002/2016JG003752
- Liu, S. M., Zhang, J., Chen, S. Z., Chen, H. T., Hong, G. H., Wei, H., et al. (2003). Inventory of nutrient compounds in the Yellow Sea. *Cont. Shelf Res.* 23, 1161–1174. doi: 10.1016/S0278-4343(03)00089-X
- Liu, X., Chiang, K.-P., Liu, S.-M., Wei, H., Zhao, Y., and Huang, B.-Q. (2015a). Influence of the Yellow Sea warm current on phytoplankton community in the central Yellow Sea. *Deep Sea Res. Part 1 Oceanogr. Res. Pap.* 106, 17–29. doi: 10.1016/j.dsr.2015.09.008
- Liu, X., Huang, B., Huang, Q., Wang, L., Ni, X., Tang, Q., et al. (2015b). Seasonal phytoplankton response to physical processes in the southern Yellow Sea. *J. Sea Res.* 95, 45–55. doi: 10.1016/j.seares.2014.10.017
- Locarnini, R. A., Mishonov, A. V., Antonov, J. I., Boyer, T. P., Garcia, H. E., Baranova, O. K., et al. (2013). *Data from: World Ocean Atlas 2013. Volume 1, Temperature*. NOAA Atlas NESDIS 73. Silver Spring, MD: National Oceanographic Data Center, 40. doi: 10.7289/V55X26VD
- Luo, L., Kao, S.-J., Bao, H., Xiao, H., Xiao, H., Yao, X., et al. (2018). Sources of reactive nitrogen in marine aerosol over the Northwest Pacific Ocean in spring. *Atmos. Chem. Phys.* 18, 6207–6222. doi: 10.5194/acp-18-6207-2018
- Menten, L., and Michaelis, M. I. (1913). Die kinetik der invertinwirkung. *Biochem. Z.* 49, 333–369.
- Morel, A., and Berthon, J. F. (1989). Surface pigments, algal biomass profiles, and potential production of the euphotic layer: relationships reinvestigated in view of remote-sensing applications. *Limnol. Oceanogr.* 34, 1545–1562. doi: 10.4319/lo.1989.34.8.1545
- Moskilde, E. (1996). *Topics in Non-Linear Dynamics: Application to Physics, Biology and Economic Systems*. Hackensack, NJ: World Scientific.
- NFRDI (2014). *Study on the Chlorosis Phenomena in Cultivated Phytopia*. Annual Report of National Fisheries Research and Development Institute. Quezon City: National Fisheries Research and Development Institute.
- Park, M., Shin, S. K., Do, Y. H., Yarish, C., and Kim, J. K. (2018). Application of open water integrated multi-trophic aquaculture to intensive monoculture: a review of the current status and challenges in Korea. *Aquaculture* 497, 174–183. doi: 10.1016/j.aquaculture.2018.07.051
- Ryther, J. H., and Dunstan, W. M. (1971). Nitrogen, phosphorous, and eutrophication in the coastal marine environment. *Science* 171, 1008–1013. doi: 10.1126/science.171.3975.1008
- Seo, G.-H., Cho, Y.-K., Choi, B.-J., Kim, K.-Y., Kim, B., and Tak, Y.-J. (2014). Climate change projection in the Northwest Pacific marginal seas through dynamic downscaling. *J. Geophys. Res. Oceans* 119, 3497–3516. doi: 10.1002/2013JC009646
- Shchepetkin, A. F., and McWilliams, J. C. (2005). The regional oceanic modeling system (ROMS): a split-explicit, free-surface, topography-following-coordinate oceanic model. *Ocean Model.* 9, 347–404. doi: 10.1016/j.ocemod.2004.08.002
- Shi, J., Liu, Y., Mao, X., Guo, X., Wei, H., and Gao, H. (2017). Interannual variation of spring phytoplankton bloom and response to turbulent energy generated by atmospheric forcing in the central Southern Yellow Sea of China: satellite observations and numerical model study. *Cont. Shelf Res.* 143, 257–270. doi: 10.1016/j.csr.2016.06.008
- Shi, W., and Wang, M. (2012). Satellite views of the Bohai Sea, Yellow Sea, and East China Sea. *Prog. Oceanogr.* 104, 30–45. doi: 10.1016/j.pocean.2012.05.001
- Shim, J. H., Hwang, J. R., Lee, S. Y., and Kwon, J. (2014). Variations in nutrients & CO₂ uptake rates of porphyra yezoensis ueda and a simple evaluation of in situ N & C demand rates at aquaculture farms in South Korea (in Korean). *Korean J. Environ. Biol.* 32, 297–305. doi: 10.11626/KJEB.2014.32.4.297
- Siswanto, E., Tang, J., Yamaguchi, H., Ahn, Y.-H., Ishizaka, J., Yoo, S., et al. (2011). Empirical ocean-color algorithms to retrieve chlorophyll-a, total suspended matter, and colored dissolved organic matter absorption coefficient in the Yellow and East China Seas. *J. Oceanogr.* 67, 627–650. doi: 10.1007/s10872-011-0062-z
- Smayda, T. J. (1969). Some measurements of the sinking rate of fecal pellets. *Limnol. Oceanogr.* 14, 621–625. doi: 10.4319/lo.1969.14.4.0621
- Song, G., Liu, S., Zhu, Z., Zhai, W., Zhu, C., and Zhang, J. (2016). Sediment oxygen consumption and benthic organic carbon mineralization on the continental shelves of the East China Sea and the Yellow Sea. *Deep Sea Res. Part 2 Top. Stud. Oceanogr.* 124, 53–63. doi: 10.1016/j.dsr2.2015.04.012
- Sun, Y.-J., and Cho, Y.-K. (2010). Tidal front and its relation to the biological process in coastal water. *Ocean Sci. J.* 45, 243–251. doi: 10.1007/s12601-010-0022-3
- Tan, S.-C., and Shi, G.-Y. (2012). The relationship between satellite-derived primary production and vertical mixing and atmospheric inputs in the Yellow Sea cold water mass. *Cont. Shelf Res.* 48, 138–145. doi: 10.1016/j.csr.2012.07.015
- Tak, Y.-J., Cho, Y.-K., and Nam, S. (2020). Numerical investigation of the generation of continental shelf waves and their role in the westward shift of the Yellow Sea Warm Current. *Prog. Oceanogr.* 187:102404. doi: 10.1016/j.pocean.2020.102404
- Tak, Y.-J., Cho, Y.-K., Seo, G.-H., and Choi, B.-J. (2016). Evolution of wind-driven flows in the Yellow Sea during winter. *J. Geophys. Res. Oceans* 121, 1970–1983. doi: 10.1002/2016JC011622
- Teague, W. J., and Jacobs, G. A. (2000). Current observations on the development of the Yellow Sea Warm Current. *J. Geophys. Res. Oceans* 105, 3401–3411. doi: 10.1029/1999JC900301
- Uda, M. (1934). Hydrographical research on the normal monthly conditions in the Japan Sea, the Yellow Sea, and the Okhotsk Sea. *J. Imp. Fish. Exp. Sta.* 5, 191–236.
- Uitz, J., Claustre, H., Morel, A., and Hooker, S. B. (2006). Vertical distribution of phytoplankton communities in open ocean: an assessment based on surface chlorophyll. *J. Geophys. Res. Oceans* 111:C08005. doi: 10.1029/2005JC003207
- Um, I. K., Choi, M. S., Bae, S. H., Song, Y., and Kong, G. S. (2018). Provenance of fine-grained sediments in the inner shelf of the Korea Strait (South Sea), Korea. *Ocean Sci. J.* 53, 31–42. doi: 10.1007/s12601-017-0062-z
- Vörösmarty, C. J., Fekete, B., and Tucker, B. A. (1996). *Data from: River Discharge Database, Version 1.0 (RivDIS v1.0), Volumes 0 through 6. A contribution to IHP-V Theme: 1. Technical Documents in Hydrology Series*. Paris: UNESCO.
- Wang, B., Wang, X., and Zhan, R. (2003). Nutrient conditions in the Yellow Sea and the East China Sea. *Estuar. Coast. Shelf Sci.* 58, 127–136. doi: 10.1016/S0272-7714(03)00067-2
- Wang, J., Beusen, A. H. W., Liu, X., Van Dingenen, R., Dentener, F., Yao, Q., et al. (2020). Spatially explicit inventory of sources of nitrogen inputs to the Yellow Sea, East China Sea, and South China Sea for the period 1970–2010. *Earth's Future* 8:e2020EF001516. doi: 10.1029/2020EF001516
- Wang, K., Chen, J. F., Jin, H. Y., Chen, F. J., Li, H. L., Gao, S. Q., et al. (2011). The four seasons nutrients distribution in Changjiang River Estuary and its adjacent East China Sea. *J. Mar. Sci.* 29, 18–35.
- Wang, Q., Guo, X., and Takeoka, H. (2008). Seasonal variations of the Yellow River plume in the Bohai Sea: a model study. *J. Geophys. Res. Oceans* 113:C08046. doi: 10.1029/2007JC004555
- Wei, Q.-S., Yu, Z.-G., Wang, B.-D., Fu, M.-Z., Xia, C.-S., Liu, L., et al. (2016). Coupling of the spatial-temporal distributions of nutrients and physical conditions in the southern Yellow Sea. *J. Mar. Syst.* 156, 30–45. doi: 10.1016/j.jmarsys.2015.12.001
- Wu, H., Gu, J., and Zhu, P. (2018). Winter counter-wint transport in the inner southwestern Yellow Sea. *J. Geophys. Res. Oceans* 123, 411–436. doi: 10.1002/2017JC013403
- Wu, Z., Yu, Z., Song, X., Wang, W., Zhou, P., Cao, X., et al. (2019). Key nitrogen biogeochemical processes in the South Yellow Sea revealed by dual stable isotopes of nitrate. *Estuar. Coast. Shelf Sci.* 225:106222. doi: 10.1016/j.ecss.2019.05.004
- Xing, Q., Yu, H., Yu, H., Sun, P., Liu, Y., Ye, Z., et al. (2020). A comprehensive model-based index for identification of larval retention areas: a case study for Japanese anchovy *Engraulis japonicus* in the Yellow Sea. *Ecol. Indic.* 116:106479. doi: 10.1016/j.ecolind.2020.106479
- Xuan, J.-L., Zhou, F., Huang, D.-J., Wei, H., Liu, C.-G., and Xing, C.-X. (2011). Physical processes and their role on the spatial and temporal variability of the spring phytoplankton bloom in the central Yellow Sea. *Acta Ecol. Sin.* 31, 61–70. doi: 10.1016/j.chnaes.2010.11.011
- Yamaguchi, H., Kim, H.-C., Son, Y. B., Kim, S. W., Okamura, K., Kiyomoto, Y., et al. (2012). Seasonal and summer interannual variations of SeaWiFS chlorophyll a in the Yellow Sea and East China Sea. *Prog. Oceanogr.* 105, 22–29. doi: 10.1016/j.pocean.2012.04.004
- Yanagi, T., and Takahashi, S. (1993). Seasonal variation of circulations in the East China Sea and the Yellow Sea. *J. Oceanogr.* 49, 503–520. doi: 10.1007/BF02237458

- Yang, H.-W., Cho, Y.-K., Seo, G.-H., You, S. H., and Seo, J.-W. (2014). Interannual variation of the southern limit in the Yellow Sea bottom cold water and its causes. *J. Mar. Syst.* 139, 119–127. doi: 10.1016/j.jmarsys.2014.05.007
- Yuan, D., Li, Y., Wang, B., He, L., and Hirose, N. (2017). Coastal circulation in the southwestern Yellow Sea in the summers of 2008 and 2009. *Cont. Shelf Res.* 143, 101–117. doi: 10.1016/j.csr.2017.01.022
- Zhang, J. (1994). Atmospheric wet deposition of nutrient elements: correlation with harmful biological blooms in Northwest Pacific coastal zones. *Ambio* 23, 464–468.
- Zhang, G., Zhang, J., and Liu, S., (2007). Characterization of nutrients in the atmospheric wet and dry deposition observed at the two monitoring sites over Yellow Sea and East China Sea. *J. Atmos. Chem.* 57, 41–57. doi: 10.1007/s10874-007-9060-3
- Zhao, B., Yao, P., Bianchi, T. S., Arellano, A. R., Wang, X., Yang, J., et al. (2018). The remineralization of sedimentary organic carbon in different sedimentary regimes of the Yellow and East China Seas. *Chem. Geol.* 495, 104–117. doi: 10.1016/j.chemgeo.2018.08.012
- Zhou, F., Chai, F., Huang, D., Xue, H., Chen, J., Xiu, P., et al. (2017). Investigation of hypoxia off the Changjiang Estuary using a coupled model of ROMS-CoSiNE. *Prog. Oceanogr.* 159, 237–254. doi: 10.1016/j.pocean.2017.10.008
- Zhou, F., Xuan, J., Huang, D., Liu, C., and Sun, J. (2013). The timing and the magnitude of spring phytoplankton blooms and their relationship with physical forcing in the central Yellow Sea in 2009. *Deep Sea Res. Part 2 Top. Stud. Oceanogr.* 97, 4–15. doi: 10.1016/j.dsr2.2013.05.001
- Zweng, M. M., Reagan, J. R., Antonov, J. I., Locarnini, R. A., Mishonov, A. V., Boyer, T. P., et al. (2013). *Data From: World Ocean Atlas 2013. Volume 2, Salinity*. NOAA Atlas NESDIS 74. Silver Spring, MD: National Oceanographic Data Center, 39. doi: 10.7289/V5251G4D
- Conflict of Interest:** The authors declare that the research was conducted in the absence of any commercial or financial relationships that could be construed as a potential conflict of interest.
- Publisher's Note:** All claims expressed in this article are solely those of the authors and do not necessarily represent those of their affiliated organizations, or those of the publisher, the editors and the reviewers. Any product that may be evaluated in this article, or claim that may be made by its manufacturer, is not guaranteed or endorsed by the publisher.
- Copyright © 2022 Tak, Cho, Hwang and Kim. This is an open-access article distributed under the terms of the Creative Commons Attribution License (CC BY). The use, distribution or reproduction in other forums is permitted, provided the original author(s) and the copyright owner(s) are credited and that the original publication in this journal is cited, in accordance with accepted academic practice. No use, distribution or reproduction is permitted which does not comply with these terms.